UNIVERSITY OF CRETE

DEPARTMENT OF CHEMISTRY

Master Thesis

General Postgraduate Programme

Synthesis of triple stimuli-responsive diblock and triblock copolymers and their self-assembly behavior

Dimitrios Gounaris Nikolaidis

Supervisors: Prof. Maria Vamvakaki

Prof. Spiros H. Anastasiadis

Heraklion 2022

ΠΑΝΕΠΙΣΤΗΜΙΟ ΚΡΗΤΗΣ

ΤΜΗΜΑ ΧΗΜΕΙΑΣ

Μεταπτυχιακο Δίπλωμα Ειδίκευσης

Γενικό Μεταπτυχιακό Πρόγραμμα Σπουδών

Σύνθεση τριπλά-αποκρίσιμων δισσυσταδικών και τρισυσταδικών συμπολυμερών και η αυτο-οργάνωσή τους

Δημήτριος Γούναρης Νικολαΐδης

Υπεύθυνοι καθηγητές: Καθ. Μαρία Βαμβακάκη

Καθ. Σπύρος Αναστασιάδης

Ηράκλειο 2022

Acknowledgments

First of all, I would like to express my profound gratitude to my supervisor Professor Maria Vamvakaki for giving me the opportunity to work and complete my master thesis in her lab. Under her continuous guidance, support and motivation i enlightened in the fields of chemistry and polymer science. She trusted my passion for polymers and gave me the chance to work in a very challenging and exciting project. I would also like to thank Professor Spiros Anastasiadis for his willingness to supervise my thesis and Professor Anna Mitraki for participating in my committee.

Special thanks to my friends inside and outside the group, G. Karantanais, N. Konios G. Karchilakis, C. Baltzaki for their support. Also I would like to express my gratitude towards the rest of the group, T. Manouras, M. Kaliva, E. Vasilaki, M. Psarrou, D. Fergadis, S. Mountaki, M. Kothris and D. Gaitanou.

My deepest appreciation goes to my girlfriend Maria Karouzou and my family, my parents with my two brothers. Their sacrifices, continuous support and love made me the person who I am today.

Abstract

Light-responsive block copolymers have attracted great interest for a variety of technological and biomedical applications, due to their remote and spatiotemporally controlled response to the external stimulus. Photo-responsive self-assembled polymer micelles have been proposed for a variety of applications, such as nanocarriers to encapsulate hydrophobic molecules within their cores and release them in response to light irradiation. In this work, multifunctional, stimuli-responsive triblock copolymers have been synthesized via reversible addition fragmentation chain transfer (RAFT) polymerization. The well-defined triblock copolymers, containing a hydrophobic spiropyran methacrylate (SPMA) block, a hydrophilic, pH- and temperature-sensitive poly(2-(dimethylamino)ethyl methacrylate) (PDMAEMA) block and a hydrophilic poly(ethylene glycol) (PEG) block, were self-assembled into spherical core-shell-corona micelles in water. The core of the micelles is sensitive to changes of the solution temperature and pH as well as to light irradiation, whereas the shell is temperature- and pH-responsive. In addition, diblock copolymers with a hydrophobic SPMA block and a hydrophilic PDMAEMA block, which self-assembled into core-shell micelles in water, were synthesized by RAFT polymerization. The response and the morphology of the copolymer micelles, upon UV and visible light irradiation, were monitored by UV/vis spectroscopy and field emission scanning electron microscopy (FESEM). This study focuses on the detailed investigation and exploitation of the adjustable polymorphism, from the nano to the micro scale, of the spiropyran-based self-assemblies.

Table of Contents

1. Introduction

1.1 Stimuli-responsive polymers

Stimuli responsive polymers or so-called “smart polymers” have been intensively studied over the past years for a diverse range of applications in nano- and bio-technology, due to their tunable structure and functionality.[1,2] These smart macromolecular chains are capable of conformational and chemical changes in response to a variety of chemical and/or physical stimuli, such as temperature,[3–5] mechanical force,[6] solution pH,[7–9] electrical or magnetic fields[6,10,11] and light irradiation[12–14] (**Figure 1**). The activated polymers undergo structural or morphological changes, such as molecular bond rearrangement/cleavage, etc, which can result in changes in their macroscopic properties, i.e., color, shape and functionality.[15] Due to the plethora of different functional groups, stimuli-responsive polymers with the desirable mechanical, optical, biological and chemical properties can be synthesized. These intelligent materials have been proposed for applications in the fields of biology, medicine, materials science, and others and can be used as sensors-biosensors, controlled drug delivery systems, etc.[1,2,16]

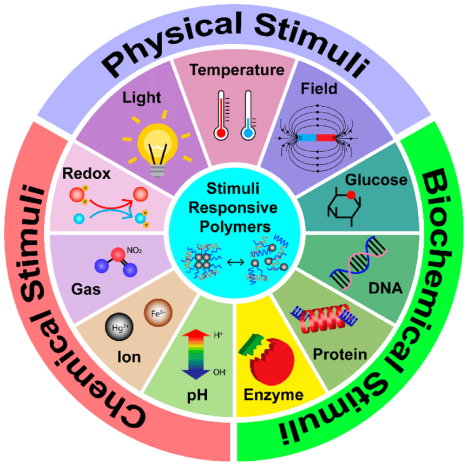

Figure 1: Physical, chemical, and biochemical triggers applied to stimuli-responsive polymers.[17]

1.2 Temperature-responsive polymers

Among all employed stimuli, temperature is among the most widely investigated. Polymers that respond to temperature are classified into two types main types depending on their response to temperature: the lower critical solution temperature (LCST) and upper critical solution temperature (UCST) polymers. Polymers that undergo a LCST phase transition are soluble in water at temperatures below the LCST and phase separate upon increasing the temperature, due to polymer-polymer intra- and inter-molecular interactions. On the other hand, UCST polymers dissolve in the solvent at temperatures above the UCST, but are insoluble at lower temperatures, due to electrostatic and/or hydrogen bonding interactions.[5,18] The most widely known LCST type polymer is poly(N-isopropylacrylamide) (PNIPAm) (**Figure 2**), which phase separates at around 32 °C and has been excessively studied for use in biological applications.[19] Another interesting and unique polymer which possesses a LCST between 32-53 °C is poly(2-(dimethylamino)-ethyl methacrylate) (PDMAEMA) (**Figure 2**). PDMAEMA responds to temperature as well as to pH changes in aqueous solution, while due to its cationic nature it can also form nanocomplexes with DNA.[20] The LCST varies depending on the polymer molecular weight, the solution pH, and the salt concentration.[21,22]

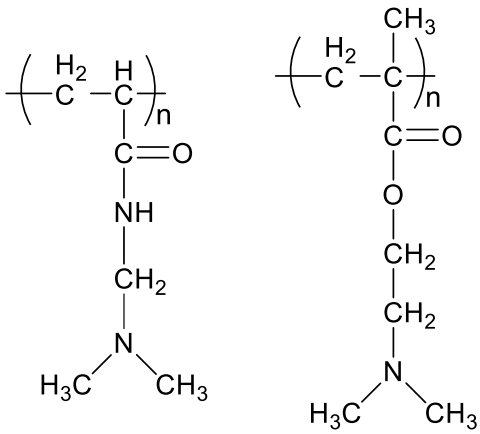

Figure 2: Polymers with LCST behavior, PNIPAm (left) and PDMAEMA (right).

1.3 pH-responsive polymers

Another extensively studied stimulus is the solution pH. pH-responsive polymers can alter reversibly their charge, solubility, volume, chain conformation and surface

activity by changing the pH of the solution. The driving force for the reversible microphase separation or the self-organization of these polymers, that is activated upon the appropriate adjustment of the solution pH, are the ionic interactions. These "smart" polymers been proposed for numerous applications in personal care, industrial coatings, controlled drug delivery, etc. The latter is very promising in particular when targeting anti-cancer drug delivery to the acidic tumors.[7] pH responsive polymers can be classified into two main types depending on the ionizable pendant groups. These are the weak polyacids and weak polybases. The polyacid pendant groups accept protons at low pH and release them at high pH, and as a result the polymers are non-ionized at low pH when the acidic groups are protonated, whereas as the solution pH increases the polymer becomes negatively charged and highly soluble in polar media.[23] The most frequently used weak polyacids are those which bear a carboxylic acid group, i.e. poly(acrylic acid) (PAA), poly(methacrylic acid) (PMAA), etc. On the other hand, polybases bear amine groups on their side groups, which become protonated at low pH values, thus increasing the internal repulsion between neighboring monomer repeat units, which leads to an overall increase of the polymer dimensions. As the pH increases, the amine groups become deprotonoted, leading to a reduction of the charge repulsion and to a decrease of the hydrodynamic size of the polymer.[24] The most frequently used polybases are: poly(2(4)-vinyl pyridine) (P2(4)VP), poly((2-diethylamino)ethyl methacrylate) (PDEA), poly((2-dimethylamino)ethyl methacrylate) (PDMAEMA) (**Figure 3**), which is also a thermo-responsive polymer, and others.

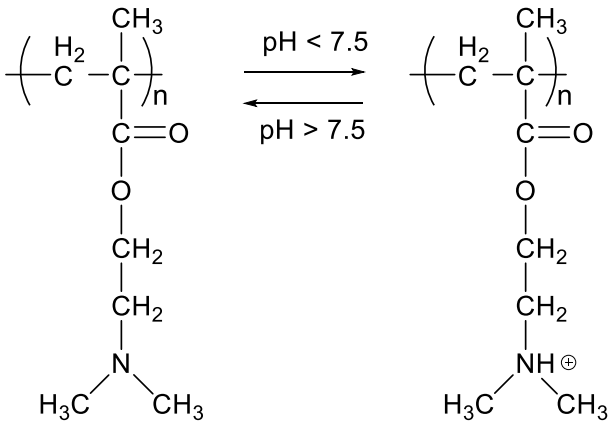

Figure 3: Protonation - deprotonation process of the PDMAEMA homopolymer.

1.4 Light-responsive polymers

Besides pH and temperature, discussed above, light irradiation has attracted great attention in the recent years as a stimulus. The unique advantages of light comprise the precise spatiotemporal and remote, nonintrusive control, the facile dosing in order to tune the strength of the response and the limitation of the chemical impurities in the system, as most of the photochemical processes do not require additional reagents.[25] Furthermore, the irradiation parameters such as the wavelength and the intensity of the light can be easily modulated to meet the system's requirements. Light-responsive behavior can either be reversible or irreversible, depending on the chromophore that is incorporated within the polymer chain. Irreversible light-responsive polymers contain photolabile units that upon irradiation can be cleaved through irreversible transformation. The most well-known light-degradable unit is the o-nitrobenzyl ester (ONB) moiety. In contrary to irreversible systems, reversible-light responsive polymers undergo a reversible photoreaction (isomerization) upon irradiation. This process can regulate the polymer properties such as the polarity, amphiphilicity, charge, optical chirality, conformation, colour, etc.[14] For the isomerization of the chromophore units, UV-light in the range between 300-400 nm, is most frequently used, while for the reversible process heat or visible light is often employed. The reversibility of these systems renders them great candidates for a variety of biomedical and technological applications, such as molecular switches, drug delivery systems, artificial muscles, actuators, etc. Several photochromic organic molecules including azobenzenes,[26,27] dithienylethenes,[28,29] anthracenes, coumarins[30,31] and spiropyrans[32–34] have been introduced into polymers to prepare light-responsive systems (**Figure 4**).

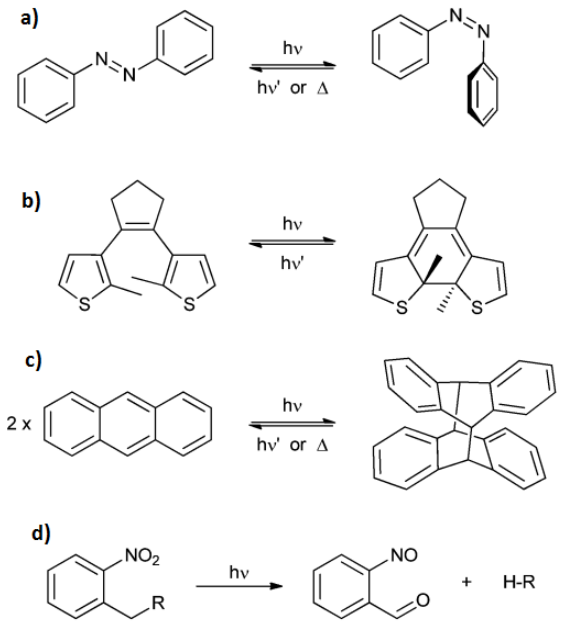

Figure 4: Photoactive chemical groups, azobenzene reversible trans–cis isomerization (a), dithienylethene reversible cyclisation (b), anthracene reversible dimerization (c) and irreversible o-nitrobenzene cleavage (d).[35]

1.4.1 Spiropyran molecules

Spiropyran compounds have had a significant impact in the emergence of the field of chromism, and since their discovery have been proposed in numerous potential applications in diverse fields. Spiropyran molecules consist of two heteroaromatic rings, one being a pyran ring connected through a sp^3 hybridized spiro C atom, as shown in **Figure 5**. Ar1 and Ar2 can represent benzene, naphthalene, anthracene, indolinol, thiophenol or other aromatic rings.[36]

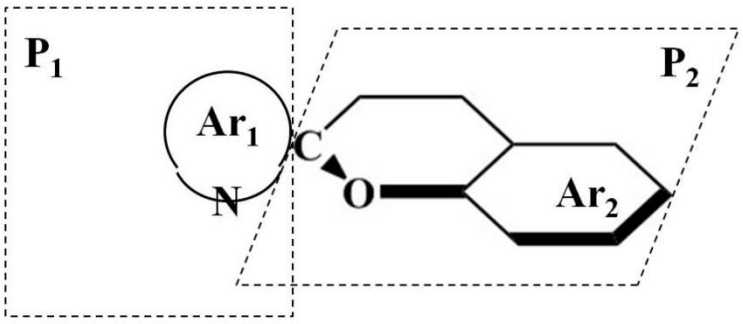

Figure 5: Basic structure of spiropyran.

The most widely investigated spiropyran is the indolinospiropyran, in which Ar1 represents an indole ring, and it was also used in this study (**Figure 6**). The two rings of the molecule are orthogonal to each other and usually the ring-closed form is called spiropyran (SP), while the ring-opened form is called merocyanine (MC). In the SP form, electron transitions exist leading to absorption peaks of these colorless molecules in the UV region. Upon UV irradiation, cleavage of the C-O bond occurs, and the non-planar rings become coplanar, while the molecule forms a large conjugated system. In contrast to the SP form, MC is polar, colored and is accompanied with a large red shift in its absorption spectra. The re-isomerization of the MC to SP form occurs either with visible light irradiation or upon heating.[37]

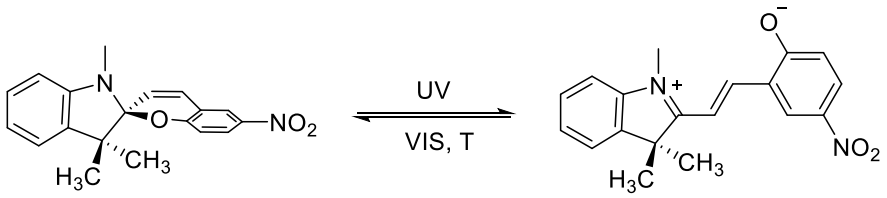

Figure 6: Reversible isomerization of spiropyran upon UV and visible light irradiation. SP form (left) and MC form (right).

1.4.2 Properties of spiropyran

The properties of spiropyran are not limited to its photochromism, since the molecule also exhibits solvatochromism, thermochromism, acidochromism, mechanochromism, etc. All these properties render spiropyrans very unique molecules, and the embodiment of a spiropyran moiety within a polymer chain leads to a multi-responsive polymer. In general, solvatochromism is the ability of a molecule to change its color due to the change in the solvent polarity. Merocyanine isomers exhibit negative solvatochromism meaning that as the polarity of the solvent increases, the absorption peaks in the visible light range is blue shifted (**Figure 7**). This effect is caused by intermolecular interactions, such as hydrogen bonding, between the solvent and the MC molecules.[37]

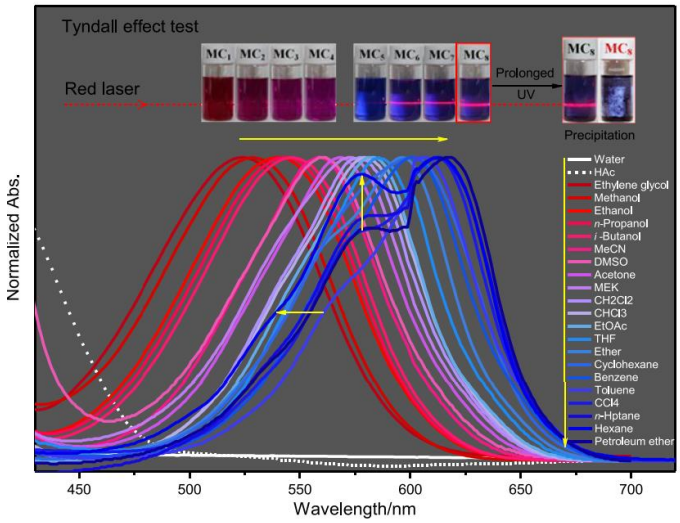

Figure 7: Effect of the solvent polarity on the absorption spectrum of merocyanine.[37]

Acidochromism is the ability of a compound to change its colour due to a charge-induced change upon ionization. In the presence of any charged species, protons in the case of acidochromism, the polar merocyanine can be stabilized in its protonated merocyanine form (MCH^+).[38] The re-isomerization of the protonated merocyanine back to the SP state can occur upon visible light irradiation (**Figure 8**).

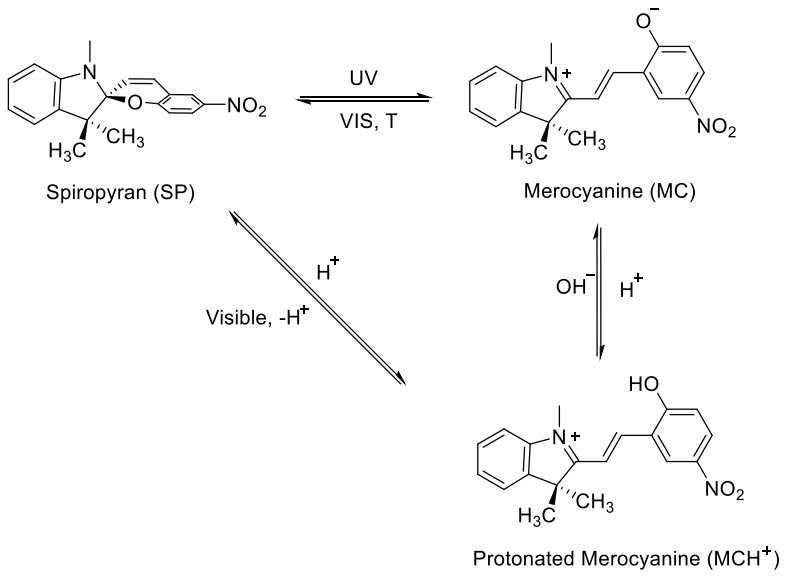

Figure 8: Acidochromism of merocyanine.

Mechanochromism is the ability of the molecules to change their shape, and thus their properties, upon application of mechanical strain or ultrasound. Similarly, when stress is applied to a spiropyran-embedded material, isomerization to the coloured MC form occurs. The stress induced ring-opening of the spiropyran molecule takes place upon application of the stress on both sides of the spiro centre, causing the cleavage of the C_{spiro}-O bond (**Figure 9**)[39].

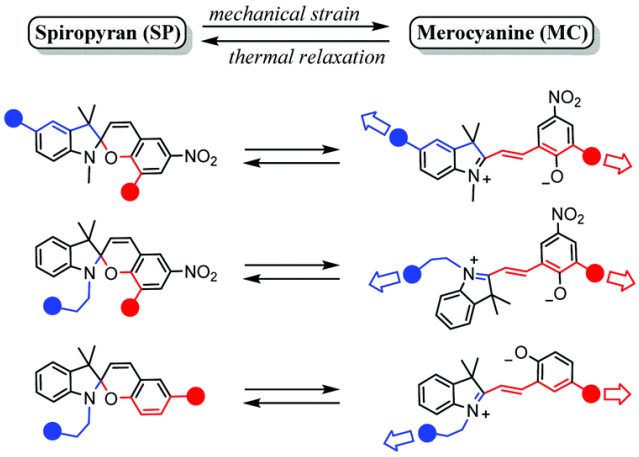

Figure 9: Substitution positions of spiropyran that enable mechanical strain.[38]

1.4.3 Merocyanine isomer

The physical changes induced in the structure of spiropyran upon UV irradiation, have a significant impact on the self-assembly behavior of the molecule, since merocyanine has unique self-assembly capabilities. The polar zwitterionic MC isomers tend to form intermolecular stacks due to dipolar and π–π stacking interactions between the molecules. The electrostatic forces compensation leads to two kinds of aggregates: the H-aggregates (antiparallel) with a head-to-tail molecular arrangement and the J-aggregates (parallel) in which molecules are arranged as bricks in a wall.[40] The control over the MC aggregates still remains a challenge, with the first report on these superstructures, that were formed by the zipper crystallization method and were named Quasi-crystals, manifesting both their crystalline and amorphous properties (**Figure 10**).[41]

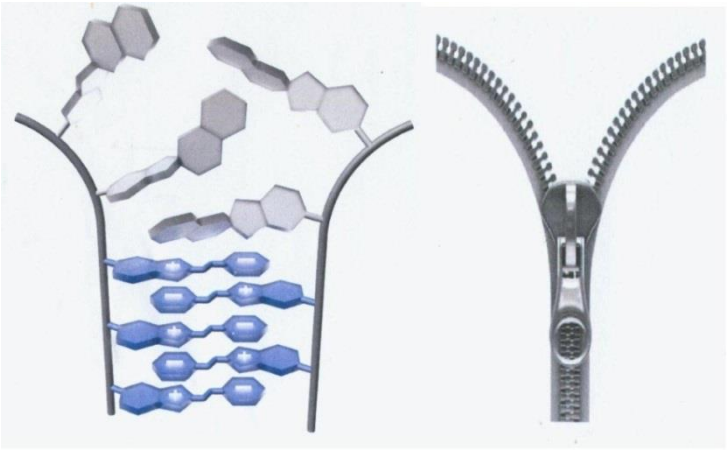

Figure 10: Self-assembly of the spiropyran polymers by zipper crystallization.[41]

1.5 Amphiphilic block copolymers

Amphiphilic block copolymers have attracted great attention over the past decades due to their unique properties and their numerous applications in medicine, nanotechnology, etc. These macromolecules comprise of two or more chemically different polymer blocks joined together by covalent bonds (**Figure 11**).[42] The synthesis of amphiphilic block copolymers occurs using living or controlled polymerization methods (anionic/cationic or radical) and more than one type of monomer species, usually one hydrophilic and one hydrophobic.[43,44] The resulting polymers possess both hydrophilic (polar) and lipophilic (non-polar) properties, and can, under certain conditions, self-assemble into energetically stable structures in order to reduce the free energy of the system and the avoid the unfavourable hydrophobe-water interactions.

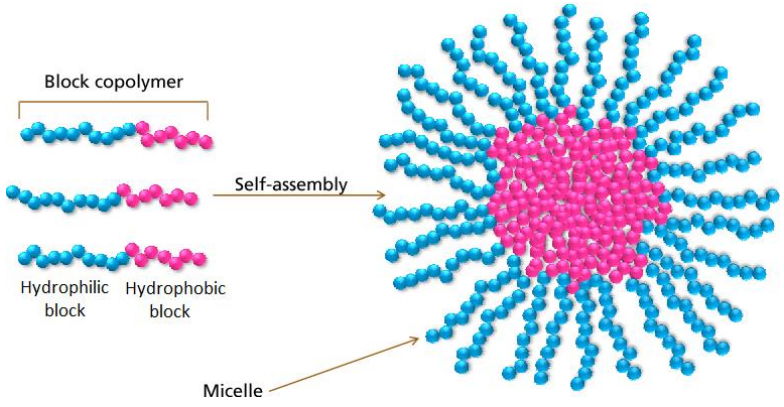

Figure 11: Self-assembly of amphiphilic diblock copolymers.[45]

1.5.1 Self-assembly of amphiphilic molecules

Self-assembly is ubiquitous in nature as systems of any size, autonomously organize into patterns or structures of reduced energy.[46–49] Molecular self-assembly involves the spontaneous organization of molecules through non-covalent interactions such as electrostatic interactions (ionic bonds), hydrogen bonds, hydrophobic/hydrophilic interactions, π–π stacking and van der Waals interactions.[48–50] The exploitation of self-assembly as a bottom-up approach provides a wide range of complex structures with desirable properties, such as micelles, vesicles, rods, etc, which can be used in various applications in many different fields.[48,51–53] Specific self-assembled nanostructures can be targeted according to a packing parameter (p) which is defined by the following equation[54]:

$$p = \frac{v}{a_o l_c}$$

Where, v is the volume of the hydrophobic block, α_o is the optimal area of the head group and l_c is the length of the insoluble hydrophobic block. As a general rule, when $p \leq 1/3$ spherical micelles are favoured, when $1/3 \leq p \leq ½$ cylindrical micelles are formed, while when $1/2 \leq p \leq 1$ enclosed membrane structures, like vesicles, can be obtained (**Figure 12**).

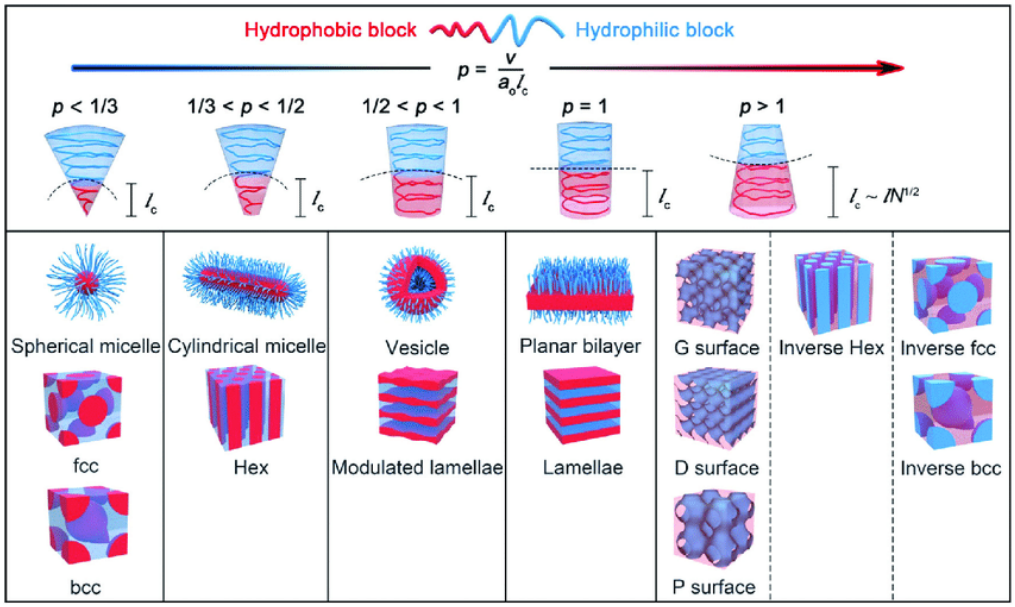

Figure 12: Self-assembled structures formed by amphiphilic diblock copolymers of different packing parameter (p).[55]

However, controlling the primary morphology of these structures or even the secondary arrangement of the molecules, which usually occurs by the application of an external stimulus, still remains a great challenge.[16,56,57]

1.5.2 Micellization - Polymer micelles

Polymer micelles are formed when the concentration of the amphiphile in the solution is above the critical micelle concentration (CMC) at a given temperature. However, the temperature of the solution must also be above the critical micellization temperature (CMT) for the formation of micelles. At concentrations below the CMC, the copolymers exist only as individual molecules (unimers) in the solution. The formation of the micelles is governed by the balance between the attractive and repulsive interactions. The attractive forces include hydrophobic and electrostatic interactions, which direct the segregation of the core segment from the aqueous phase. On the other hand, steric interactions and electrostatic repulsion contribute to the repulsive forces and prevent the unlimited growth of the micelles.[58] Polymeric micelles are usually composed of hundreds of molecules with a typical diameter around 100 nm and narrow size distribution.

There are different kinds of micelles, the core-shell micelles with a hydrophobic core and a hydrophilic shell (**Figure 13a and c**), the reverse micelles (**Figure 13b**) with a hydrophilic core and a hydrophobic shell, and the micelles that consist of double-hydrophilic block copolymers (DHBC), known as core-shell-corona micelles (**Figure 13d**). In recent years the development of core-shell-corona micelles has attracted great attention, in comparison to the diblock and symmetric triblock copolymers, due to the different morphologies that have been observed in the nanometer scale. These micelles consist of asymmetric triblock copolymers with the third block used to introduce additional control properties and thus influencing the self-assembly process and the stability of the micelles.[59,60]

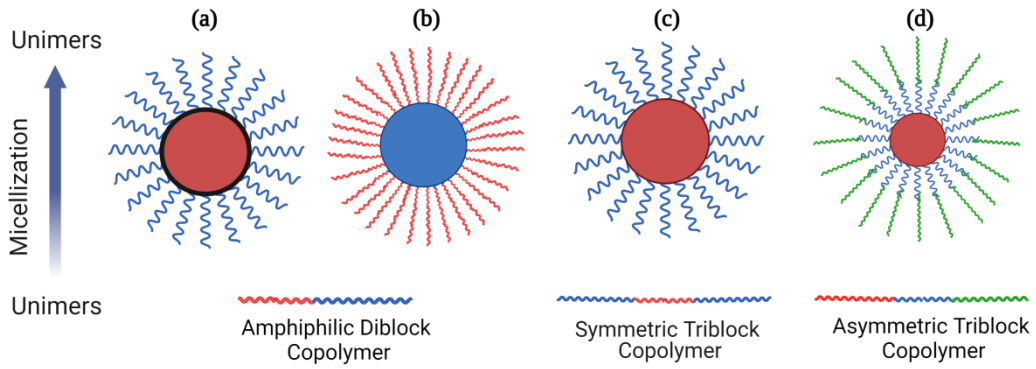

Figure 13: Formation of polymer micelles from different types of block copolymers.

1.6 Stimuli-responsive micelles

The self-assembly of stimuli-responsive amphiphilic block copolymers results in stimuli-responsive micelles with advanced properties. These structures can be used in various applications, due to their response to external stimuli such as temperature, pH, light irradiation, etc. The response to one or more stimuli could change drastically the properties of the micelles and even cause their disruption. As a result, many of these systems have been investigated as drug delivery vehicles.

1.7 Reversible addition fragmentation chain transfer (RAFT) polymerization

Reversible addition fragmentation chain transfer polymerization has become one of the most versatile and powerful techniques for the synthesis of complex polymer architectures including block, star and comb (co)polymers. RAFT polymerization enables the control over the molecular weight and molecular weight distribution of the polymer, while it also provides living characteristics to the polymer chains. The polymerization process involves, a thiocarbonylthio group (S=C-S) with substituents R and Z, as the chain transfer agent (CTA) that impacts the polymerization reaction kinetics and therefore, the degree of structural control.[61] The RAFT mechanism is shown in **Figure 14**.

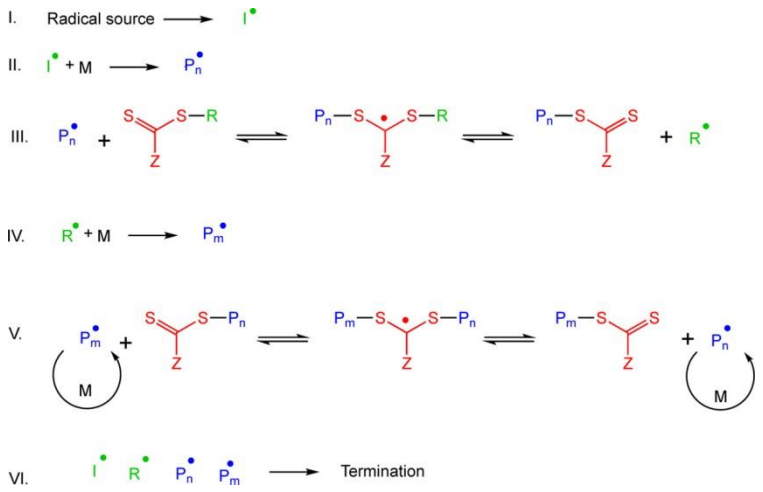

Figure 14: Proposed mechanism of RAFT polymerization.[61]

A key for the successful polymerization is the equilibrium between the active propagating radicals (Pn· and Pm·) and the dormant polymeric thiocarbonylthio species. The rate of the addition/fragmentation equilibrium must be faster than the propagation, ensuring that all the polymer chains grow with the same possibility. Additionally, the re-initiation and propagation should also be fast enough to suppress the termination. However, the selection of appropriate CTAs for different classes of monomers is a critical factor for the enhanced control in RAFT polymerization (**Figure 15**).

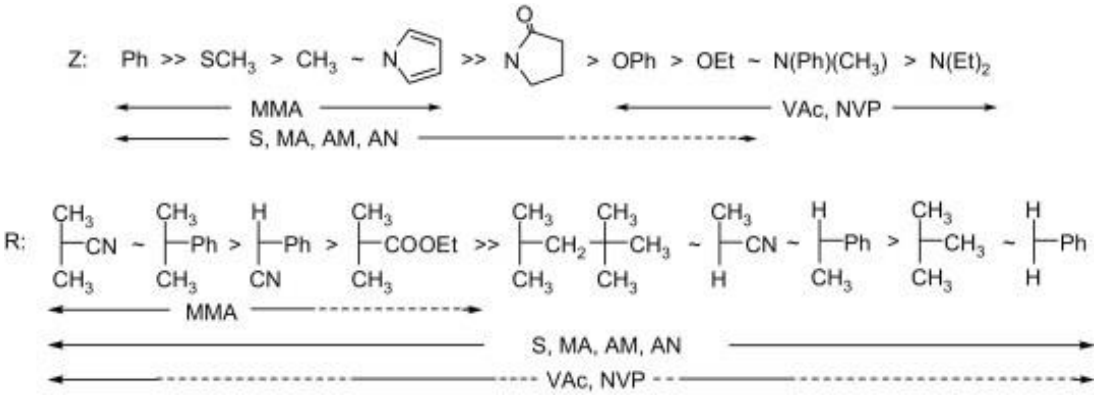

Figure 15: Guidelines for the selection of appropriate RAFT agents for the polymerization of different monomer classes.[62]

The Z-group is primarily responsible for the C═S bond reactivity towards radical addition and controls the stability of the intermediate radical, which must be weighed against the propagating radical reactivity. On the other hand, the R-group has to be a good leaving group, but also rapidly initiate propagation to ensure all chains are initiated early in the reaction to achieve a narrow molecular weight distribution.[62]

For the purpose of this work a suitable CTA for the polymerization of methacrylate monomers had to be chosen. 4-cyano-4-[(dodecylsulfanylthiocarbonyl)sulfanyl] pentanoic acid (CDTPA) (**Figure 16**) is commonly used in the literature as a CTA for the polymerization of methacrylate monomers and was thus selected.

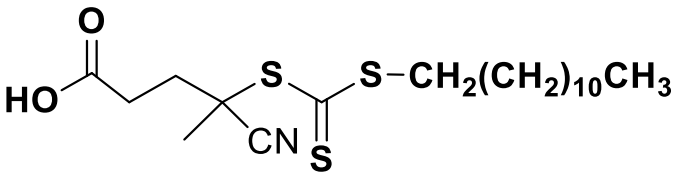

Figure 16: Chemical structure of the 4-cyano-4-[(dodecylsulfanylthiocarbonyl) sulfanyl]pentanoic acid chain transfer agent.

2. Experimental Section

2.1 Materials

DMAEMA (Aldrich, 98%) was passed through a basic alumina column prior to polymerization. 2,2′-azobis(2-methylpropionitrile) (AIBN, Aldrich, 98%), 4-cyano-4-[(dodecylsulfanylthiocarbonyl)sulfanyl] pentanoic acid (CDTPA, Aldrich, 97%), 2-bromoethanol (Aldrich, 95%), 2,3,3-trimethylindolenine (Aldrich, 98%), 2-hydroxy-5-nitrobenzaldehyde (Aldrich, 98%), dicyclohexylcarbodiimide (DCC, Aldrich, 99%), 4-(dimethyl122 amino)pyridine (DMAP, Aldrich, ≥99%), potassium hydroxide, 1,4-dioxane (Carlo Erba, 99.8%), petroleum ether (Aldrich, 99%), toluene (Aldrich, ≥99.7%), triethylamine (TEA, Aldrich, ≥99.5%), 2-propanol (Aldrich, ≥99.5%), and hexane (Aldrich, 95%) were used as received. Milli-Q water of specific resistivity of 18.2 MΩ·cm at 25 °C was used in all experiments.

2.2 Synthesis of spiropyran methacylate (SPMA)

2.2.1 Synthesis of 1-(2-hydroxyethyl)-2,3,3-trimethyl-3H-indolium bromide

In a two-neck flask, bearing a side arm and equipped with a condenser, a mixture of 2,3,3-trimethyl-3H-indole (8.9 g, 0.056 mol) and 2-bromoethanol (8.75 g, 0.07 mol) in dry acetonitrile (75 mL) was refluxed at 100 °C for 72 h under an inert nitrogen atmosphere (Scheme 1). After cooling down to ambient temperature, the solvent was evaporated under reduced pressure to obtain a dark red solid. The crude solid product was suspended via sonication and underwent several washing cycles with hexane. The product was further purified with n-hexane and $CHCl_3$ (2:1), and with diethyl ether and methanol (3:1) to remove the unreacted reagents. It was next isolated via filtration and dried under reduced pressure. The dark pink solid, still containing traces of the initial reactants, was then recrystallized several times from chloroform to obtain 13.5 g of the pink pure product, 1-(2-hydroxyethyl)-2,3,3-trimethyl-3H-indolium bromide, in 85 % yield, which was further characterized by ^{1}H NMR spectroscopy in D_2O.

2.2.2 Synthesis of 9,9,9a-trimethyl-2,3,9,9a-tethadydro-oxazolo[3,2-α]indole

1-(2-hydroxyethyl)-2,3,3-trimethyl-3H-indolium bromide (13.6 g, 0.047 mol) were dissolved in 235 mL water for 2 h. Then, potassium hydroxide (4.2 g, 0.075 mol) was added to the pink solution and was further reacted for 4 h at room temperature, under continuous stirring. The yellow oily product, which phase separated in the aqueous medium, was extracted with diethyl ether (4 × 90 mL). The volume of the organic phase was reduced under reduced pressure and stirred over anhydrous magnesium sulfate to remove traces of water. Next, the solution was filtered and the solvent was evaporated to obtain 9,9,9a-trimethyl-2,3,9,9a-tethadydro-oxazolo[3,2-α]indole (9.5 g) as a yellow oil at 99 % yield, which was characterized by ^{1}H NMR spectroscopy in $CDCl_3$.

2.2.3 Synthesis of 1'-(2-hydroxyethyl)-3',3'-dimethyl-6-nitrospiro(2H-1-benzopyran-2,2'-indoline)

In a two-neck flask, bearing a side arm and equipped with a condenser, a mixture of 9,9,9a-trimethyl-2,3,9,9a-tethadydro-oxazolo[3,2-a]indole (9.5 g, 0.047 mol) and 2-hydroxy-5-nitrobenzaldehyde (9.3 g, 0.056 mol) in EtOH (100 mL) was refluxed at 100 °C for 3 h under an inert nitrogen atmosphere. After cooling down to ambient temperature the mixture was filtered and the resulting dark purple solid was washed with EtOH (50mL) and dried under reduced pressure to obtain 1'-(2-hydroxyethyl)-3',3'-dimethyl-6-nitrospiro(2H-1-benzopyran-2,2'-indoline) (8.1 g) as purple crystals in 64 % yield, which was further characterized by ^{1}H NMR spectroscopy in $CDCl_3$.

2.2.4 Synthesis of 1´-(2-methacryloxyethyl)-3',3´-dimethyl-6-nitrospiro-(2H1-benzopyran-2,2´-indoline) (SPMA)

The spiropyran monomer, SPMA, was synthesized via a typical Steglich esterification reaction. In a flask bearing a side arm a solution of DCC (2.46 g, 0.012 mol) in dry dichloromethane (DCM) (65 mL) was cooled to 0 °C while stirring under an inert nitrogen atmosphere. Next, methacrylic acid (MAA) (0.95 mL, 0.011 mol) was added to the reaction. After 10 min, 4-dimethylaminopyridine (DMAP) (0.25 g, 0.002 mol),

which acts as a catalyst was transferred in the reaction mixture and was further reacted with SP-OH (3 g, 0.0085 mol) to obtain the final ester. The reaction was allowed to proceed for 2 days at RT in the absence of light. Next, the crude product was isolated under reduced pressure and was purified via column chromatography (silica gel, $CHCl_3$). It was recrystallized several times from methanol to afford 2.2 g (0.0052 mol) of light green powder in 61 % yield, which was further characterized by ^{1}H NMR spectroscopy in $CDCl_3$. Due to the SP-to-MC ring-opening reaction of the monomer upon interaction with acidic silica, the silica column was first packed with the same solvent mixture used for the molecule elution in the presence of 7% triethylamine (TEA) to reduce the acidity of the packing material.

2.3 Synthesis of 2-(8-(hydroxymethyl)-3′,3′-dimethyl-6-nitrospiro[chromene 2,2′-indolin]-1′-yl)ethanol (Bifunctional spiropyran)

2.3.1 Synthesis of 3-hydroxymethyl-5-nitrosalicylaldehyde

In a two-neck flask, bearing a side arm and equipped with a condenser, 3-chloromethyl-5-nitrosalicylaldehyde (1 g, 4.54 mmol) was dissolved in an acetone/nanopure water mixture (5.5 mL/1.8 mL) under an inert N_2 atmosphere. After heating to reflux temperature for 20 min, aqueous sodium hydroxide (0.8 mL of a 6 M solution) was added dropwise over a period of 3 min. The reaction mixture was stirred and refluxed for 3 h and after cooling down to ambient temperature the crude product was isolated under reduced pressure. Next, chloroform was added and the mixture was filtered to isolate the byproducts. The solution was then precipitated from hexane to afford 0.3 g (1.5 mmol) of a light green powder in 33% yield, which was further characterized by ^{1}H NMR spectroscopy in $CDCl_3$.

2.3.2 Synthesis of 2-(8-(hydroxymethyl)-3′,3′-dimethyl-6-nitrospiro[chromene2,2′-indolin]-1′-yl)ethanol

In a two-neck flask, bearing a side arm and equipped with a condenser, a mixture of 9,9,9a-trimethyl-2,3,9,9a-tethadydro-oxazolo[3,2-a]indole (0.3 g, 1.48 mmol) and 3-

hydroxymethyl-5-nitrosalicylaldehyde (0.150 g, 0.392 mmol) in EtOH/H_2O (10 mL) was refluxed at 90 °C for 5 h under an inert nitrogen atmosphere. After cooling down to ambient temperature the crude product was isolated under reduced pressure and washed with 70% aqueous acetonitrile solution and two times with diethyl ether to remove the unreacted reagents. Next, the product was dried under reduced pressure to obtain 0.03 g (0.078 mmol) purple crystals in 20%, yield which was further characterized by ^{1}H NMR spectroscopy in $CDCl_3$.

2.4 Synthesis of the PEG-*b*-PDMAEMA-*b*-PSPMA triblock copolymer

2.4.1 Synthesis of the macromolecular chain transfer agent mPEG$_{112}$-CDTPA (macro-CTA)

The PEG macro-RAFT agent was synthesized by a typical esterification reaction. In a flask bearing a side arm, a mixture of poly(ethylene glycol) methyl ether M_n = 5000 g/mol (5 g, 0.001 mol) and 4-cyano-4-[(dodecylsulfanylthiocarbonyl)sulfanyl] pentanoic acid (CDTPA) (0.807 g, 0.002 mol) in dry dichloromethane (DCM) (25 mL) was cooled to 0 °C, while stirring under an inert nitrogen atmosphere. Next, a mixture of DCC (0.413 g, 0.002 mol) and DMAP (0.029 g, 0.24 mmol) in dry DCM (2 mL) was transferred dropwise in the reaction over a period of 2 min. The reaction was allowed to proceed for 2 days at 40 °C. Next, the reaction mixture was filtered in order to remove the byproduct (dicyclohexyl urea) that was formed during the esterification reaction. The crude product was purified by repeated precipitations (four times) into diethyl ether and subsequent dissolution into CH_2Cl_2. The final product was dried under reduced pressure to obtain mPEG$_{112}$-CDTPA (4.63 g) as a yellow powder in 86% yield, which was further characterized by ^{1}H NMR spectroscopy in $CDCl_3$.

2.4.2 Synthesis of the poly[(ethylene glycol)methyl ether]-*b*-poly[2-(dimethylamino)ethyl methacrylate] macro-CTA

A typical RAFT procedure for the synthesis of the diblock copolymers using azobisisobutyronitrile (AIBN) as the initiator and $mPEG_{112}$-CDTPA as the CTA (CTA:AIBN = 10:1 mole ratio) is described below. In a dry round bottom flask bearing a side arm, $mPEG_{112}$-CDTPA (1 g, 0.185 mmol) was dissolved in 1,4-dioxane (10 mL) under an inert nitrogen atmosphere. Next, DMAEMA (1.04 g, 6.588 mmol) was added to the flask followed by the addition of AIBN (3.94 mg, 0.0185 mmol, as a solution in dioxane). The final solution was degassed by four freeze-pump-thaw cycles and subsequently placed in a preheated oil bath at 65 °C for 28 h. Next, the polymerization was terminated by cooling the solution with liquid nitrogen and exposing it to air. The diblock copolymer was isolated by precipitation in a large excess of n-hexane and was dried under reduced pressure for 24 h before being used for the polymerization of spiropyran.

2.4.3 Synthesis of the PEG-*b*-PDMAEMA-*b*-PSPMA triblock copolymer

The synthesis of the triblock copolymer was conducted using the above synthesized PEG-*b*-PDMAEMA macro-CTA (CTA:AIBN = 3:1 mole ratio) for the polymerization of the photo-responsive SPMA. A similar procedure was followed, using AIBN as the initiator and 1,4-dioxane as the solvent. In a dry round bottom flask bearing a side arm, PEG-*b*-PDMAEMA (0.5 g, 0.05 mmol) was dissolved in 1,4-dioxane (5 mL) under an inert nitrogen atmosphere. Next, SPMA (0.3 g, 0.71 mmol) was added to the flask followed by the addition of AIBN (2.74 mg, 0.0167 mmol, as a solution in dioxane). The final solution was degassed by four freeze-pump-thaw cycles and subsequently placed in a preheated oil bath at 70 °C for 24 h in the absence of light. Next, the polymerization was terminated by cooling the solution with liquid nitrogen and exposing it to air. The triblock copolymer was isolated by precipitation in a large excess of n-hexane twice, followed by dissolution in THF and drying under reduced pressure.

2.4.4 End group modification of the PEG-*b*-PDMAEMA-*b*-PSPMA triblock copolymer

In a round bottom flask bearing a side arm, PEG-*b*-PDMAEMA-*b*-PSPMA (0.1 g, 0.0067 mmol) was dissolved in toluene (2 mL) followed by the addition of AIBN (0.027 g, 0.167 mmol). The final solution was degassed by four freeze-pump-thaw cycles and subsequently placed in a preheated oil bath at 80 °C for 2.5 h in the absence of light. Next, the reaction was terminated by cooling the solution with liquid nitrogen and exposing it to air. The triblock copolymer was isolated by precipitation in a large excess of n-hexane twice, followed by dissolution in toluene and drying under reduced pressure.

2.4.5 Preparation of the triblock copolymer micelles

Polymer micelles were prepared by a typical procedure as follows: 5 mg of the amphiphilic PEG-*b*-PDMAEMA-*b*-PSPMA were dissolved in 1 mL acetonitrile, which is a good solvent for all blocks. 9 mL of nanopure water were added dropwise under vigorous stirring at room temperature. Next, the volume of the solution was reduced using a rotary evaporator, during which step the organic solvent was also evaporated, and the final polymer concentration was adjusted to 0.05 wt%. The solution was filtered through a hydrophilic 0.45 μm syringe filter before being analysed.

2.5 Synthesis of the PDMAEMA-*b*-PSPMA diblock copolymer

2.5.1 Synthesis of the poly[2-(dimethylamino)ethyl methacrylate] macro-CTA

A typical RAFT procedure for the synthesis of the PDMAEMA macro-CTA using azobisisobutyronitrile (AIBN) as the initiator and CDTPA as the CTA (CTA:AIBN = 7:1 mole ratio) is described below. In a dry round bottom flask bearing a side arm, CDTPA (0.2 g, 0.495 mmol) was dissolved in 1,4-dioxane (12mL) under an inert nitrogen atmosphere. Next, DMAEMA (7.23 g, 0.046 mol) was added to the flask followed by the addition of AIBN (11.62 mg, 0.071 mmol, as a solution in dioxane). The final solution was degassed by four freeze-pump-thaw cycles and was

subsequently placed in a preheated oil bath at 70 °C for 28 h. Next, the polymerization was terminated by cooling the solution with liquid nitrogen and exposing it to air. The homopolymer was isolated by precipitation in a large excess of n-hexane and was dried under reduced pressure for 24 h, before being used for the polymerization of spiropyran.

2.5.2 Synthesis of the PDMAEMA-*b*-PSPMA diblock copolymer

The synthesis of the PDMAEMA-*b*-PSPMA diblock copolymer was conducted using the above synthesized PDMAEMA-CDTPA as the macro-CTA (CTA: AIBN = 3:1 molar ratio) for the polymerization of the photo-responsive SPMA. A similar procedure was followed, using AIBN as the initiator and 1,4-dioxane as the solvent. In a dry round bottom flask bearing a side arm, PDMAEMA (0.5 g, 0.05 mmol) was dissolved in 1,4-dioxane (6 mL) under an inert nitrogen atmosphere. Next, SPMA (0.3 g, 0.71 mmol) was added to the flask followed by the addition of AIBN (2.74 mg, 0.0167 mmol, as a solution in dioxane). The final solution was degassed by four freeze-pump-thaw cycles and was subsequently placed in a preheated oil bath at 70 °C for 28 h in the dark. Next, the polymerization was terminated by cooling the solution with liquid nitrogen and exposing it to air. The diblock copolymer was isolated by several precipitations in a large excess of n-hexane, followed by dissolution in THF and drying under reduced pressure.

2.5.3 End-group modification of the PDMAEMA-*b*-PSPMA diblock copolymer

In a round bottom flask bearing a side arm, PDMAEMA-*b*-PSPMA (0.25 g, 0.017 mmol) was dissolved in toluene (3 mL) followed by the addition of AIBN (0.068 g, 0.416 mmol). The final solution was degassed by four freeze-pump-thaw cycles and was subsequently placed in a preheated oil bath at 80 °C for 2.5 h in the absence of light. Next, the reaction was terminated by cooling the solution with liquid nitrogen and exposing it to air. The diblock copolymer was isolated by precipitation in a large excess of n-hexane twice, followed by dissolution in toluene and drying under reduced pressure.

2.5.4 Preparation of the diblock copolymer micelles

Polymer micelles were prepared by a typical procedure as follows: 5 mg of the amphiphilic PDMAEMA-*b*-PSPMA diblock copolymer were dissolved in 1 mL isopropanol, which is a good solvent for both blocks. 9 mL of nanopure water were added dropwise under vigorous stirring at room temperature. Next, the volume of the solution was reduced using rotary evaporator, during which step the organic solvent was also evaporated, and the final polymer concentration was adjusted to 0.05 wt%. The solution was filtered through a hydrophilic 0.45 μm filter before being used.

2.6 Characterization Techniques

Size Exclusion Chromatography (SEC)

The number average molecular weights (M_n's) and the molecular weight distributions (M_w/M_n's) of the polymers were determined by size exclusion chromatography (SEC). The instrument was equipped with a Waters 515 HPLC pump (Waters, Milford, MA, USA), two PL mixed-D and mixed-E columns operated at 35 °C and a Waters 410 refractive index detector (Waters, Milford, MA, USA). The eluent was THF, containing 2 v/v% triethylamine, at a flow rate of 1 $mL \cdot min^{-1}$. The system was calibrated using a series of six narrow molecular weight linear poly(methyl methacrylate) standards, ranging from 850 to 342,900 $g\ mol^{-1}$.

Nuclear Magnetic Resonance (NMR) Spectroscopy

^1H NMR spectra were obtained on a Bruker DPX-300 spectrometer (Bruker, Rheinstetten, Germany). All samples were dissolved in chloroform-d_3 or deuterium oxide-d_2, depending on their solubility, and the spectra were recorded at RT.

Ultraviolet-Visible (UV/Vis) Spectroscopy

The SP-to-MC isomerization of the diblock and triblock copolymers was monitored, as a function of irradiation time, using a Shimadzu 2600i spectrophotometer in the

wavelength range 300−700 nm. For this purpose, the absorption spectra of 0.01 wt % aqueous solutions of the PDMAEMA-*b*-PSPMA and PEG-*b*-PDMAEMA-*b*-PSPMA copolymers were recorded following irradiation with UV or visible light.

Field Emission Scanning Electron Microscopy (FESEM)

The morphology of the self-assembled structures was studied by FESEM (JEOL JSM 7000F) at an accelerating voltage 10-30 kV. For the measurement, one drop of a dilute suspension of the polymeric solution was dropped on a glass substrate prior to drying at room temperature.

Dynamic Light Scattering (DLS)

The size of the self-assembled structures in aqueous media was measured by a Malvern Zetasizer NanoZS 90 instrument equipped with a 4 mW He-Ne laser operating at λ = 632.8 nm The scattered light intensity was measured at a scattering angle of 90°. Data were collected over a period of 2–10 min at room temperature. The reported data are the average values from triplicate measurements

Light Sources

The UV light source that was used for the isomerization of the spiropyran moiety to the merocyanine form (MC) was a Spectroline hand-held UV lamp operating at 365 nm (8 watt). The visible light source was a Variac Cermax 300 W Xenon lamp (λ > 320 nm) and a filter was used to eliminate all irradiation below 400 nm. The cuvettes containing the polymer solutions were aligned at a distance of 5 cm from the light source, ensuring the homogeneous irradiation of the sample.

3. Results and Discussion

3.1 Synthesis and characterization of spiropyran methacrylate (SPMA)

The synthesis of the spiropyran methacrylate (SPMA) monomer was achieved by a four-step reaction according to the procedure adapted from Raymo et al[63], starting from 2,3,3-trimethyl-3H-indole (**Figure 17**). Briefly, the alkylation of 2,3,3-trimethyl-3H-indole with 2-bromoethanol gave the indolium bromide salt (1) in 85% yield, while treatment of the latter with a strong base (KOH) afforded the oxazole derivative in 93% yield (2). Next the condensation of the cyclic precursor with 2-hydroxy-5-nitrobenzaldehyde under reflux for several hours produced the nitro-substituted chromophore (3, SP-OH) in 68% yield. Finally, the photochromic monomer was prepared by a Steglich esterification reaction of the spiropyran alcohol (3) with methacrylic acid in the presence of a catalyst (DMAP) and was obtained in 60% yield.

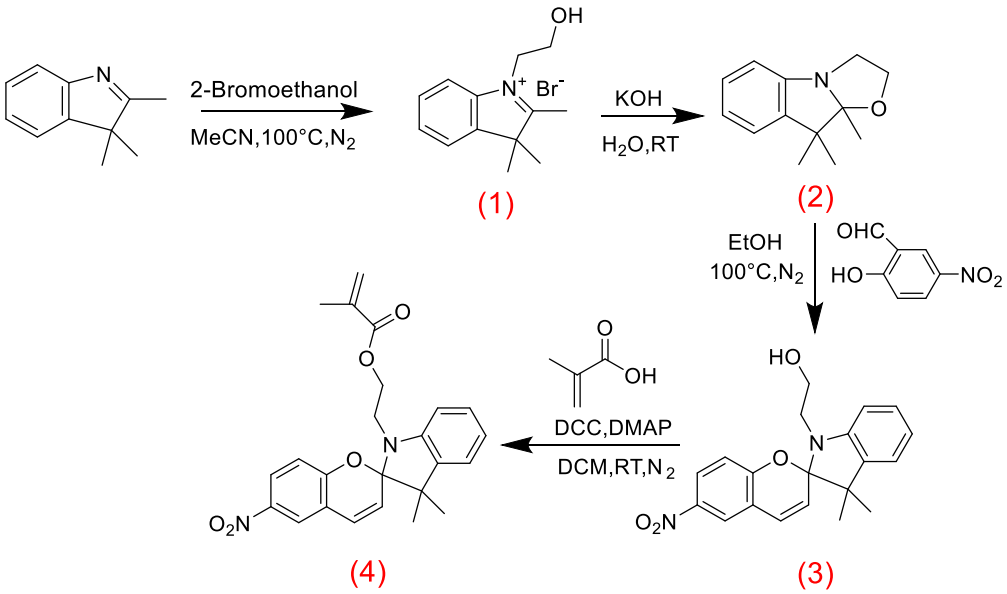

Figure 17: Synthetic route followed for the preparation of spiropyran methacrylate (SPMA).

3.1.1 Synthesis of 1-(2-hydroxyethyl)-2,3,3-trimethyl-3H indolium bromide

In the first step, the reflux of 2,3,3-trimethyl-3H-indole with 2-bromoethanol in dry acetonitrile under an inert atmosphere resulted in the pink bromide salt, 1-(2-hydroxyethyl)-2,3,3-trimethyl-3H-indolium bromide (1). The successful synthesis of 1-(2-hydroxyethyl)-2,3,3-trimethyl-3H-indolium bromide was studied by ^{1}H NMR spectroscopy in D_2O. The appearance of two new signals, at 4.08-4.11 ppm and 4.62-4.65 ppm, which are attributed to the methylene protons of the attached hydroxyethyl moiety, verified the successful alkylation of the indoline molecule. The ^{1}H NMR spectrum exhibited six signals as assigned below: (300 MHz, D_2O) δ 1.57 (6H, H-6), 2.82 (3H, H-5), 4.08-4.11 (2H, H-7), 4.62-4.65 (2H, H8), 7.61-7.64 (2H, H-1, H-2), 7.73-7.77 (2H, H-3, H-4) (**Figure 18**).

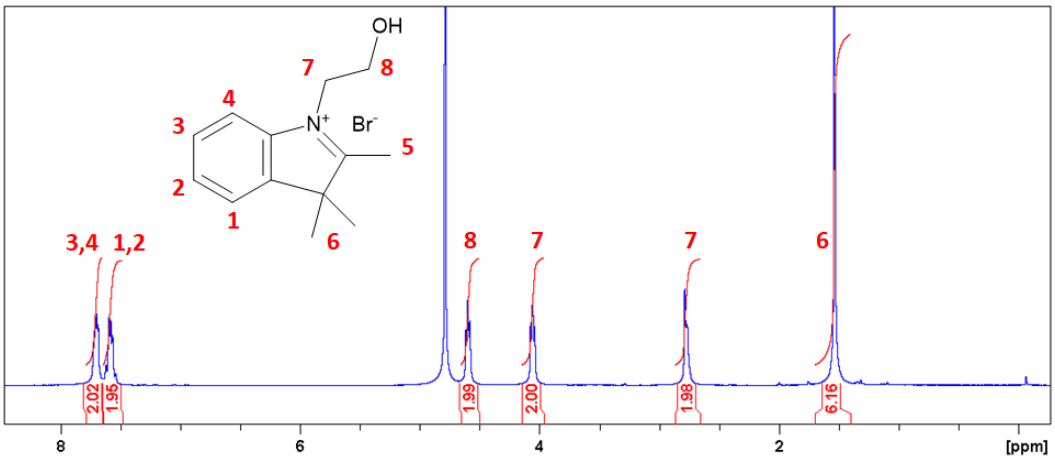

Figure 18: ^{1}H NMR spectrum of 1-(2-hydroxyethyl)-2,3,3-trimethyl-3H indolium bromide (1) in D_2O.

3.1.2 Synthesis of 9,9,9α-trimethyl-2,3,9,9α-tethadydrooxazolo[3,2-α]indole

The reaction of 1-(2-hydroxyethyl)-2,3,3-trimethyl-3H-indolium bromide with KOH in water and the formation of the cyclic product, 9,9,9α-trimethyl-2,3,9,9α-tethadydrooxazolo[3,2-α]indole (2), had a distinct effect on the ^{1}H NMR chemical shifts of the former molecule. First, the upfield shift of the two complex multiplets for the two pairs of methylene protons (H-7, 3.55 ppm, H-8, 3.8 ppm), and the upfield shift of H-5 at 1.11 ppm, demonstrated the formation of the five-membered ring which caused a change in the environment of the methyl and methylene groups. In

addition, the upfield shift of the methyl protons H-6, which were split into two singlets at 1.30 ppm and 1.34 ppm, verified the successful formation of the oxazole derivative. (300 MHz, $CDCl_3$): δ 1.19 (3H, H-5), 1.39 (3H, H-6), 1.43 (3H, H-6“), 3.48-3.63 (2H, H-7), 3.70-3.87 (2H, H-8), 6.75-6.78 (1H, H4), 6.90-6.95 (1H, H-2), 7.07-7.17 (3H, H-1, H-3) (**Figure 19**).

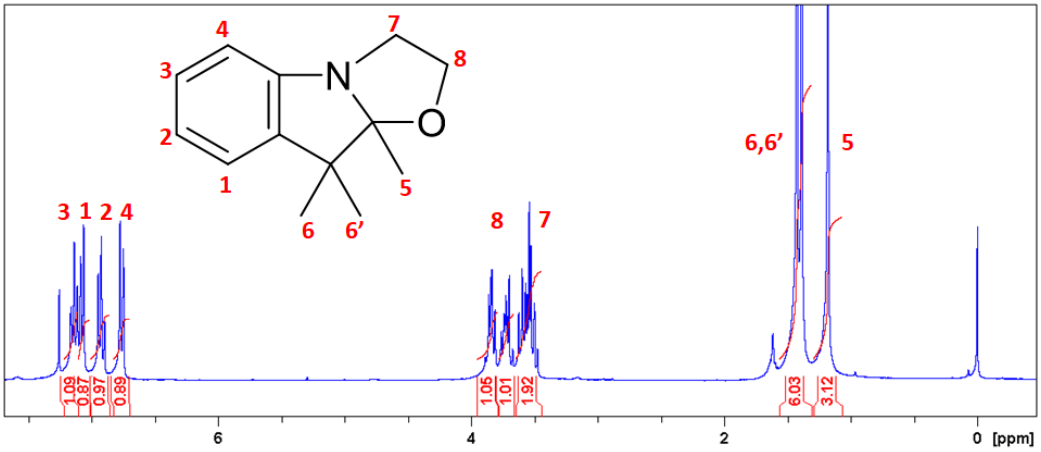

Figure 19: ^{1}H NMR spectrum of 9,9,9α-trimethyl-2,3,9,9α-tethadydrooxazolo[3,2- α]indole (2) in $CDCl_3$.

3.1.3 Synthesis of 2-(3',3'-dimethyl-6-nitro-3'H-spiro[chromene-2,2'-indol]-1'-yl)-ethanol

The synthesis of the nitro-substituted spiropyran alcohol was accomplished upon the condensation of the synthesized 9,9,9α-trimethyl-2,3,9,9α-tethadydrooxazolo[3,2-α]indole (2) with 2-hydroxy-5-nitrobenzaldehyde in ethanol under reflux temperature. The formation of a chiral spirocenter which connects the indoline and the benzopyran rings has a prominent effect on the ^{1}H NMR chemical shifts of the former molecule. The appearance of five new signals at 7.98-8.08 ppm (H-5, H-7), 7.15-7.18 ppm (H-8), 6.66-6.74 ppm (H-4) and 5.98-6.01 ppm (H-3), indicate the successful synthesis of the spiropyran derivative. Also, the change in the chemical environment led to an upfield shift of the H-9, H-10 and H-3' protons. (300 MHz, $CDCl_3$): δ 1.16 (3H, H-3'), 1.25 (3H, H-3'), 3.17-3.37 (2H, H- 9), 3.51-3.69 (2H, H10), 5.98-6.01 (1H, H-3), 6.66-6.74 (1H, H-4), 6.81-6.86 (1H, H- 7"), 7.01-7.05 (2H, H-6", H-5"), 7.10-7.12 (1H, H-4"), 7.15-7.18 (1H, H-8) and 7.98-8.08 (2H, H-5, H-7) (**Figure 20**).

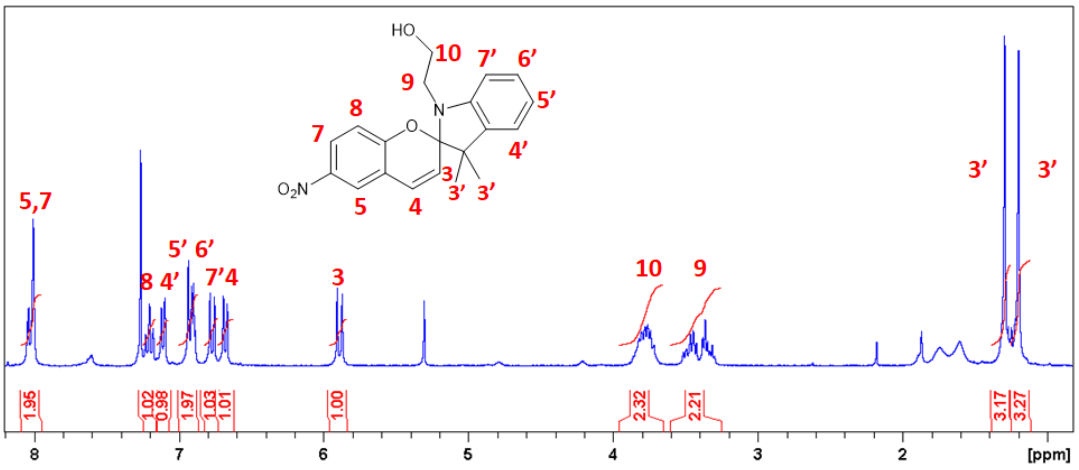

Figure 20: ^{1}H NMR spectrum of SP-OH (3) in $CDCl_3$.

3.1.4 Synthesis of spiropyran methacrylate (SPMA)

The synthesis of spiropyran methacrylate (SPMA) was accomplished via a Steglich esterification reaction of the precursor spiropyran alcohol with methacrylic acid in the presence of DCC, catalyzed by DMAP. The esterification process led to the appearance of three new signals in the ^{1}H NMR spectrum: at 5.5 ppm and 6.0 ppm, which corresponds to the protons of the carbon-carbon double bond, H-11, and a peak at 1.91 ppm assigned to the methyl group of the methacrylate moiety, H-12. In addition, the change in the chemical environment shifted the H-9 and H-10 protons downfield due to the formation of the ester group (300 MHz, $CDCl_3$): δ 1.16 (3H, H-3'), 1.28 (3H, H-3'), 1.91 (3H, H-12), 3.38-3.60 (2H, H-9), 4.28- 4.32 (2H, H-10), 5.56 (1H, H-11), 5.86-5.89 (1H, H-3), 6.07 (1H, H-11), 6.69- 6.76 (2H, H-4, H-7'), 6.88-6.92 (2H, H-5', H-6'), 7.08-7.10 (1H, H-4), 7.18-7.23 (1H, H-8), 8.0- 8.04 (2H, H-5, H-7) (**Figure 21**).

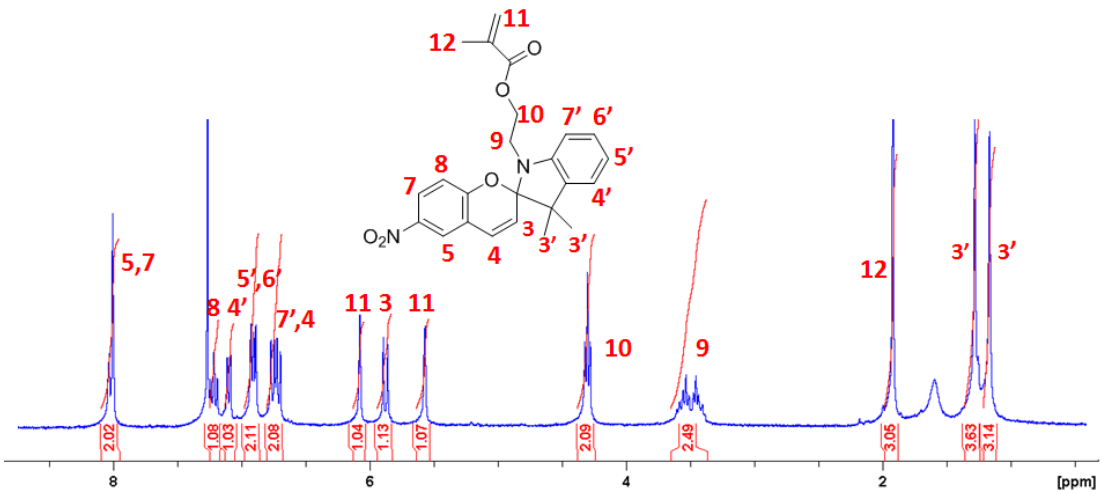

Figure 21: ^{1}H NMR spectrum of 1′-(2-methacryloxyethyl)-3′,3′- dimethyl-6-nitrospiro-(2H-1-benzopyran-2,2′-indoline) (SPMA) in $CDCl_3$.

3.2 Synthesis of 2-(8-(hydroxymethyl)-3',3'-dimethyl-6-nitrospiro[chromene 2,2'-indolin]-1'-yl)ethanol (Bifunctional spiropyran)

The synthesis of the bifunctional spiropyran derivative was achieved by a four-step reaction starting from 2,3,3-trimethyl-3H-indole, according to the procedure adapted from Raymo, F., et al. and O'Bryan, G., et al.[63,64] (**Figure 22**). Briefly, the alkylation of 2,3,3-trimethyl-3H-indole with 2-bromoethanol gave the indolium bromide salt (1) in 86% yield, while treatment of the latter with a strong base (KOH) afforded the oxazole derivative (2) in 92% yield. Next the hydrolysis of 3-chloromethyl-5-nitrosalicylaldehyde with aqueous sodium hydroxide (NaOH) produced 3-hydroxymethyl-5-nitrosalicylaldehyde (3) in 33% yield. Finally, the bifunctional spiropyran moiety was obtained by the condensation of the cyclic precursor (2) with the hydroxyl derivative (4) in 20% yield.

The first two steps of the reaction were described above in Sections 3.1.1 and 3.1.2.

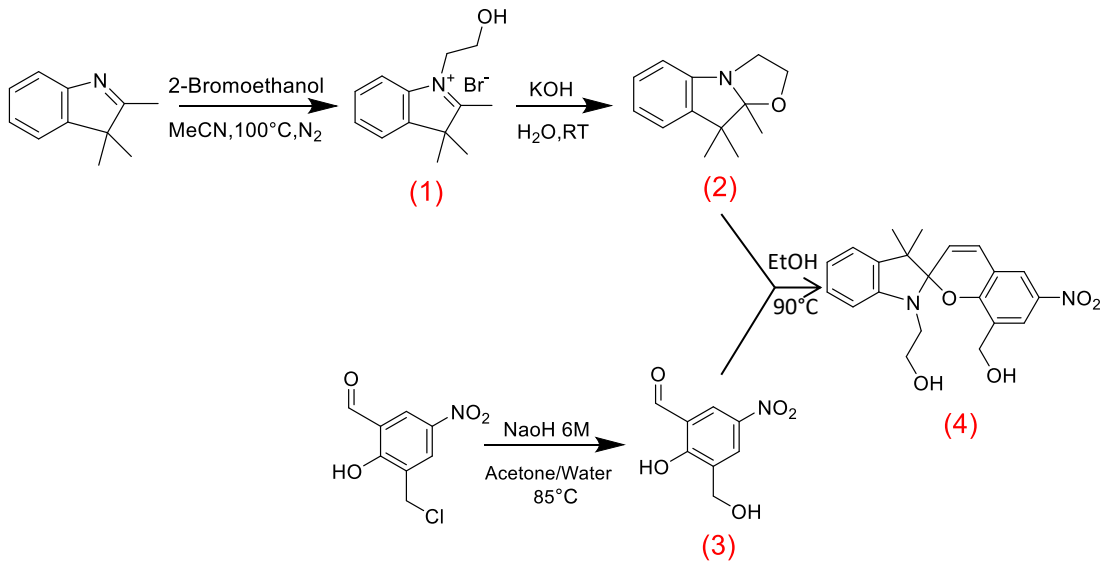

Figure 22: Synthetic route for the preparation of the bifunctional spiropyran derivative.

3.2.1 Synthesis of 3-hydroxymethyl-5-nitrosalicylaldehyde

The reaction of 3-chloromethyl-5-nitrosalicylaldehyde with aqueous sodium hydroxide (6 M NaOH) under reflux temperature and the formation of the hydroxyl derivative, 3-hydroxymethyl-5-nitrosalicylaldehyde (3), had a distinct effect on the ^{1}H NMR chemical shifts of the former molecule. The downfield shift of the methylene protons H-4 (4.87 ppm), due to the change in the chemical environment after the hydrolysis reaction, indicates the successful formation of the hydroxy derivative. ^{1}H NMR (300 MHz, $CDCl_3$) δ: 10.24 (1H, H-1), 8.62-8.72 (2H, H-2, H-3) 4.82 (2H, H-4) (**Figure 23**).

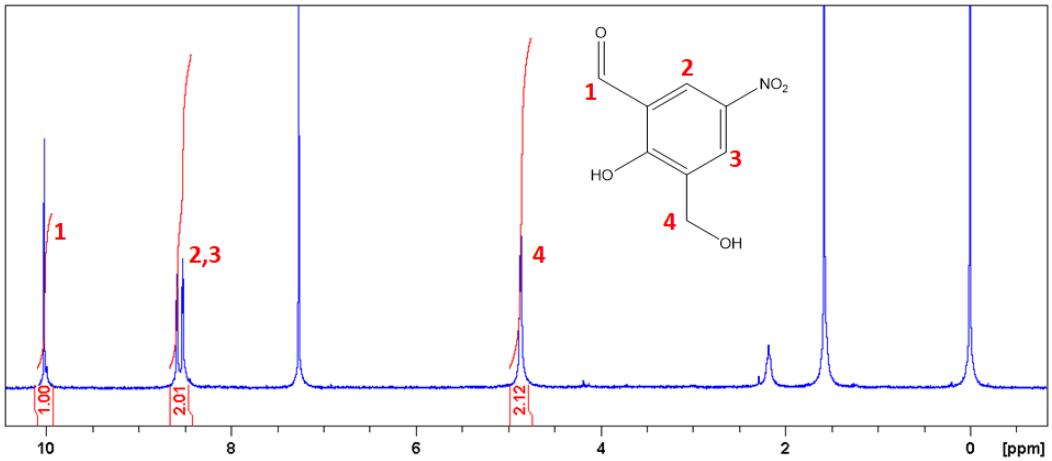

Figure 23: ^{1}H NMR spectrum of 3-hydroxymethyl-5-nitrosalicylaldehyde (3) in $CDCl_3$.

3.2.2 Synthesis of the bifunctional spiropyran derivative

The synthesis of the dihydroxy-substituted spiropyran derivative was accomplished by the condensation of the synthesized 9,9,9α-trimethyl-2,3,9,9α-tethadydrooxazolo[3,2- α]indole (2) with the synthesized 3-hydroxymethyl-5-nitrosalicylaldehyde in ethanol under reflux temperature. The formation of a chiral spirocenter, which connects the indoline and the hydroxy benzopyran ring had a prominent effect on the ^{1}H NMR chemical shifts of the former molecules. The appearance of three new signals at 7.99-8.13 ppm (H-7), 7.13-7.20 ppm (H-5) and 5.87-5.92 ppm (H-6) indicated the successful synthesis of the spiropyran derivative. In addition, the change in the chemical environment, due to the formation of the chiral spirocenter, led to an upfield shift for the H-8 and H-9 protons which appeared as two complex multiplets. (300 MHz, $CDCl_3$): δ 1.16-1.35 (6H, H-1), 3.25-3.53 (2H, H-9), 3.70-3.81 (2H, H-10), 4.36-4.64 (2H, H-8), 5.87-5.92 (1H, H-6), 6.61-6.70 (1H, H-3), 6.85-7.00 (2H, H-2), 7.05-7.13 (1H, H-4), 7.13-7.22 (1H, H-5) and 7.99-8.13 (2H, H-7) (**Figure 24**).

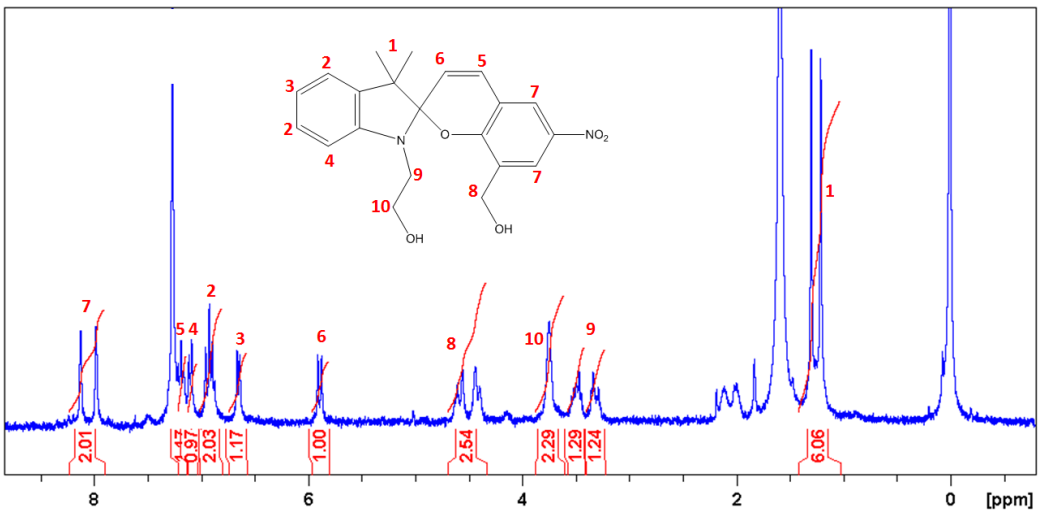

Figure 24: ^{1}H NMR spectrum of 2-(8-(hydroxymethyl)-3',3'-dimethyl-6-nitrospiro[chromene-2,2'-indolin]-1'-yl)ethanol (4) in $CDCl_3$.

3.3 Synthesis and characterization of the PDMAEMA-*b*-PSPMA diblock copolymers

3.3.1 Synthesis of the PDMAEMA homopolymer

The diblock copolymer was synthesized via radical addition-fragmentation chain transfer (RAFT) polymerization (**Figure 25**). First, the PDMAEMA-CDTPA macroinitiator was synthesized using 4-cyano-4-[(dodecylsulfanylthiocarbonyl) sulfanyl]pentanoic acid as the chain transfer agent (CTA) and azobisisobutyronitrile (AIBN) as the initiator in 1,4-dioxane at 65 °C for 28 h (**Figure 25, Step 1**). The successful polymerization was verified by SEC and ^{1}H NMR spectroscopy. The monomodal SEC curve (**Figure 26, black line**) indicates the controlled growth of the polymer chains. Namely, the resulting number average molecular weight and molecular weight distribution of the PDMAEMA macroinitiator were found M_n = 11500 g/mol and M_w/M_n = 1.13, respectively.

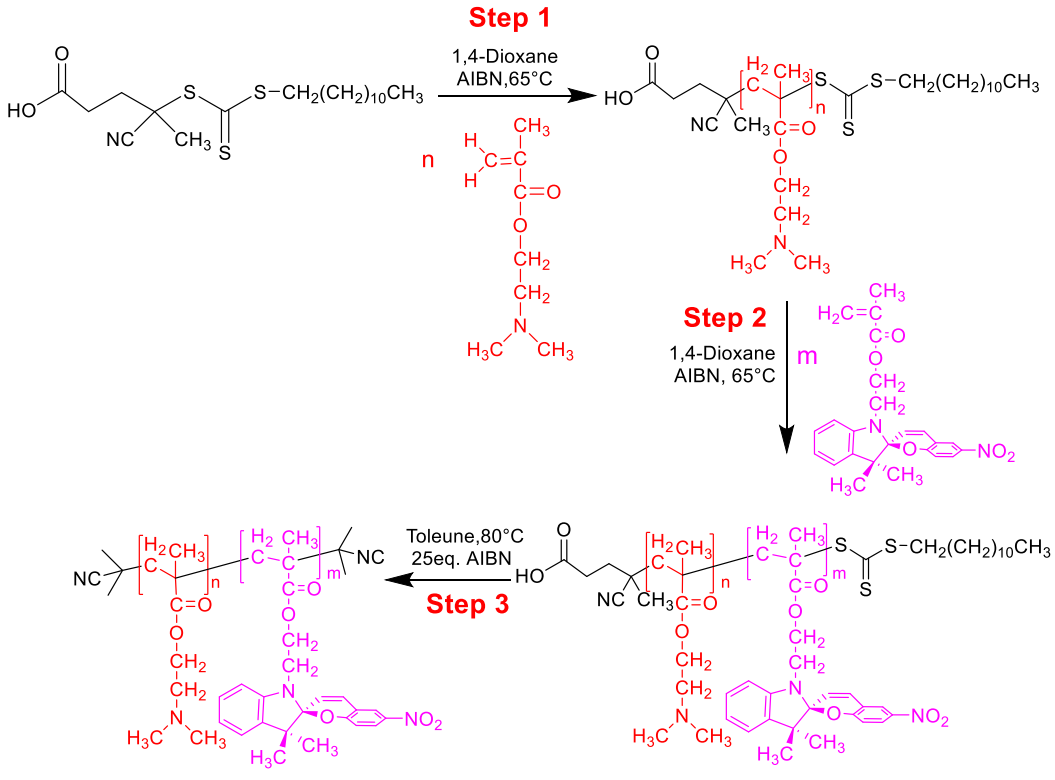

Figure 25: Synthetic route followed for the preparation of the PDMAEMA-*b*-PSPMA diblock copolymers.

3.3.2 Synthesis of the PDMAEMA-*b*-PSPMA diblock copolymer

The synthesized PDMAEMA-CDTPA macroinitiator was used for the polymerization of SPMA using azobisisobutyronitrile (AIBN) as the initiator in 1,4-dioxane at 70 °C for 28 h (**Figure 25, Step 3**). The successful polymerization was verified by SEC and ^{1}H NMR spectroscopy. The monomodal SEC curve (**Figure 26, red line**) shifted towards lower elution times, without any traces of the PDMAEMA macroinitiator, thus indicating the controlled growth of the polymer chains, as well as the living character of the polymerization. Namely, the resulting number average molecular weight and molecular weight distribution of the PDMAEMA-*b*-PSPMA diblock copolymer were found M_n = 15500 g/mol and M_w/M_n = 1.15, respectively. The ^{1}H NMR spectrum showed the characteristic peaks attributed to both the PDMAEMA and PSPMA blocks, allowing to calculate the chemical composition of the copolymers (**Figure 27, top spectrum**). The molar ratio of the two blocks, PDMAEMA and PSPMA, was determined by ratioing the peak integrals of the signal at 7.88 ppm (Ar-*H*, H-a,b) attributed to the PSPMA block and the signal at 2.56 ppm (C*H*$_2$-N, H-w) due to the PDMAEMA block. The mole ratio of the two blocks PDMAEMA/PSPMA was calculated 10:1, which corresponds to a SPMA content of 9 mol% and a 25 wt% of the SPMA block in the diblock copolymer.

3.3.3 End group modification of the diblock copolymers

The end group modification of the synthesized diblock copolymer took place using an excess of AIBN in toluene at 80 °C for 3 h (**Figure 25, Step 3**). The successful polymer modification was verified by ^{1}H NMR spectroscopy (**Figure 27, bottom spectrum**). The integral of the peaks at 0.5-1.5 ppm, in which the methyl and methylene protons of the CDTPA appeared, decreased after the modification reaction indicating the loss of the polymer end groups. Furthermore, the appearance of a new peak at 1.56 (H-p'), which corresponds to the methyl protons of the AIBN fragment ((C*H*$_3$)$_2$CN) that is attached at the polymer chain end, confirms the successful polymer derivatization.

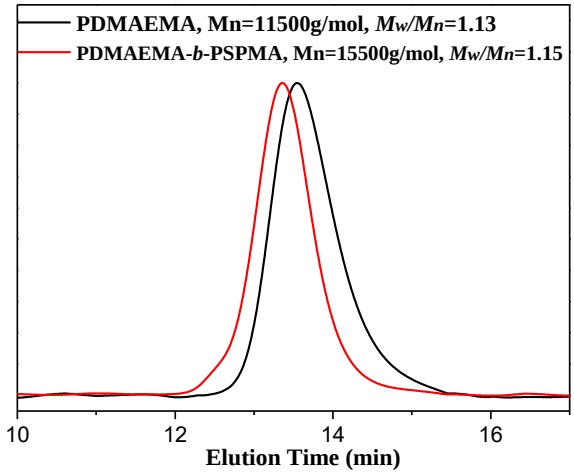

Figure 26: SEC traces of the PDMAEMA homopolymer (black line) and the PDMAEMA-*b*-PSPMA diblock copolymer (red line).

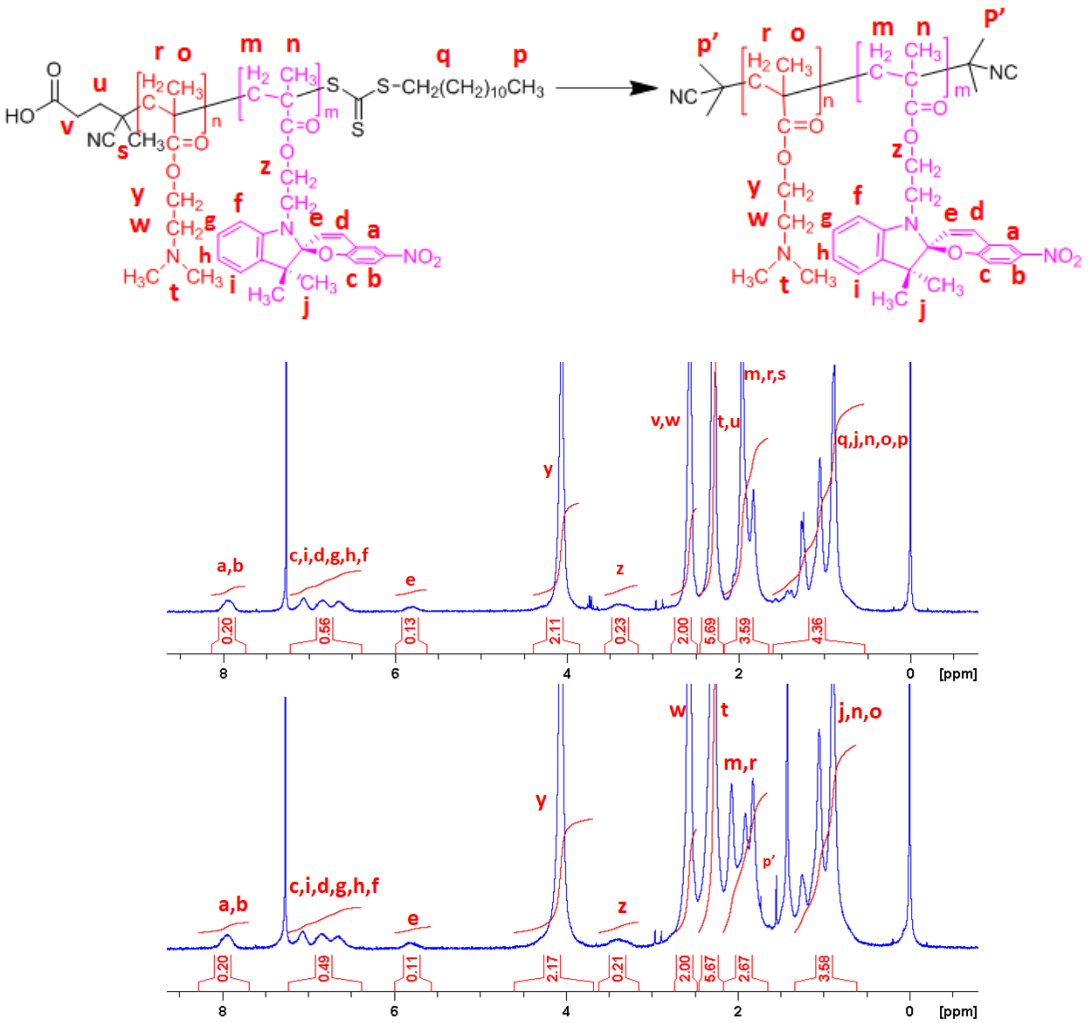

Figure 27: ^{1}H NMR spectra of the PDMAEMA-*b*-PSPMA diblock copolymer, before (top spectrum) and after (bottom spectrum) the end group modification reaction, in $CDCl_3$.

3.4 Photo-responsive properties of the PDMAEMA-*b*-PSPMA diblock copolymer in aqueous media

The photo-responsive behavior of the diblock copolymer in aqueous media was monitored by UV/Vis spectroscopy. The absorption spectra of the diblock copolymer as a function of irradiation time, with UV light at λ = 365 nm, are shown in **Figure 28**. Before UV irradiation, the absorption at λ > 450 nm is relatively low, suggesting that the PSPMA block is in the spiropyran form. The ring-opening isomerization of SP to MC was confirmed by a constant increase in the absorption band from 450 to 650 nm, after UV irradiation of the sample. The maximum isomerization of SP to MC was achieved after 25 min UV irradiation, and was also accompanied by a spontaneous change in the color of the sample, from colorless to light purple, due to the formation of the MC isomer. In parallel, an increase of the absorption between 370 nm and 440 nm was observed, which was assigned to the non-planar isomer X. It is worth noting that the peak assigned to the polar MC moieties was red-shifted from 576 to 562 nm as a function of irradiation time, possibly suggesting the formation of MC-MC aggregates.

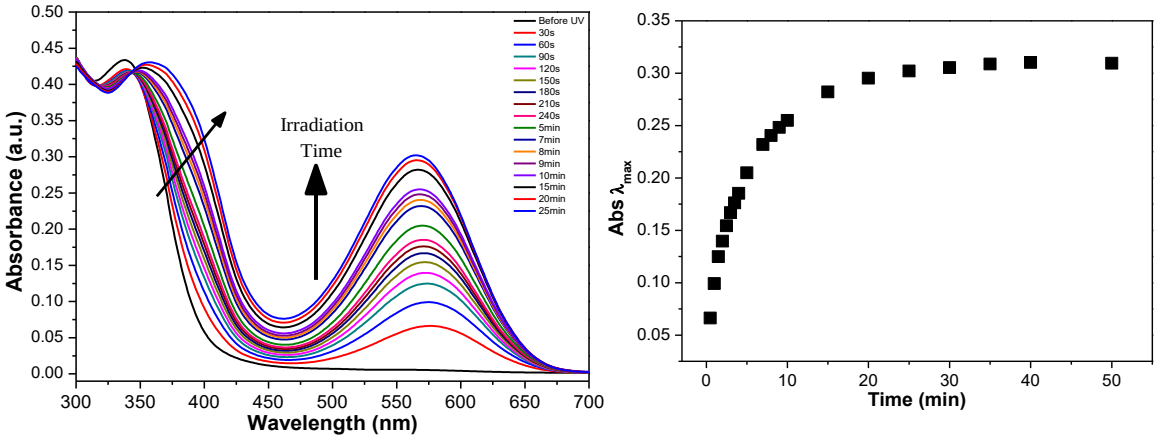

Figure 28: **Left:** UV/Vis absorption spectra of an aqueous PDMAEMA-*b*-PSPMA copolymer solution upon irradiation with UV light. **Right:** Increase of the absorption intensity of MC, at λ_{max}, as a function of irradiation time.

Next, the sample irradiated for 25 min with UV light was used to conduct a kinetic study of the isomerization of MC back to the SP form upon visible light irradiation. (**Figure 29)** shows the time-dependent change in the absorption spectra for the diblock copolymer as a function of irradiation with visible light. The absorption band of MC (450 nm-650 nm) gradually decreased, however, even after 90 min of irradiation with visible light a notable absorption was observed, suggesting that some MC isomers remain in the copolymer, and thus the MC-to-SP isomerization presents a hysteresis with irradiation time. It was found that even after prolonged irradiation, the MC isomer does not fully isomerize back to the SP form, and the system reaches a photostationary state with a mixture of the low energy closed SP form and the energetically most stable transoid open MC form.[38] Moreover, as the absorption intensity of merocyanine gradually decreased, a slight blue-shift of the MC absorption band, from 565 to 568 nm, was observed and in parallel a decrease of the absorption band of the non-planar X isomer (370 nm – 440 nm) was evident, suggesting a reversible light activated process.

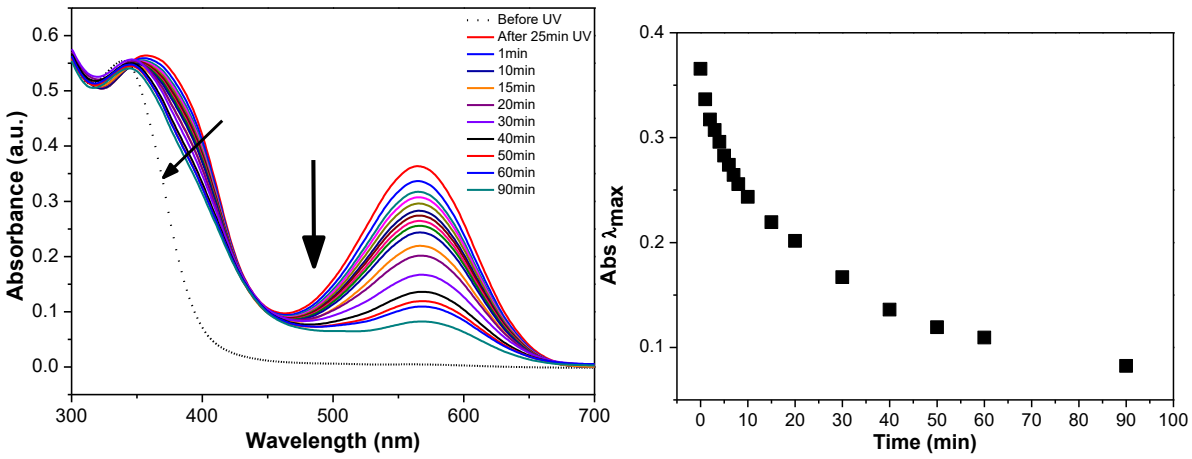

Figure 29: **Left:** UV/Vis absorption spectra of an aqueous PDMAEMA-*b*-PSPMA copolymer solution upon visible light irradiation. **Right:** Decrease of the absorption intensity of MC, at λ_{max}, as a function of irradiation time.

3.5 Self-assembly behavior of the PDMAEMA-*b*-PSPMA diblock copolymer in aqueous media

The diblock copolymer comprising a hydrophobic photo-, pH- and temperature-sensitive poly(spiropyran methacrylate) (PSPMA) block, a hydrophilic, pH- and temperature-sensitive poly(2-(dimethylamino)ethyl methacrylate)) (PDMAEMA) block, was self-assembled into micelles in water. The morphology and the size of the copolymer micelles, upon UV and visible light irradiation, were monitored by FESEM and DLS. After the micellization process, the polymer concentration was adjusted to c = 0.0025 wt%, and a drop of the solution was deposited on the silicon wafer and was dried overnight at room temperature for use in FESEM. The FESEM images revealed spherical micelles with diameter D = 117 ± 31 nm (**Figures 30a-c**). The size of the micelles in the solution was also examined using dynamic light scattering (**Figure 30d**). The average hydrodynamic diameter of the diblock copolymer micelles was found D_h = 90 nm, which is in relatively good agreement with the size determined by FESEM. To investigate the stability of the micelles in the aqueous medium, a sample was measured again by DLS after 3 weeks, and the hydrodynamic diameter was found almost identical to the initial size, proving the excellent stability of the nanostructures.

Next, the micellar copolymer solution was placed in a quartz cuvette and was irradiated with UV light for 25 min prior to FESEM observation. The images of the UV irradiated sample in FESEM showed the formation of a thin film with shapeless structures (**Figure 31**). From these images it was concluded that the isomerization of the hydrophobic spiropyran moieties to the hydrophilic merocyanine isomer has led to the disruption of the micelles.

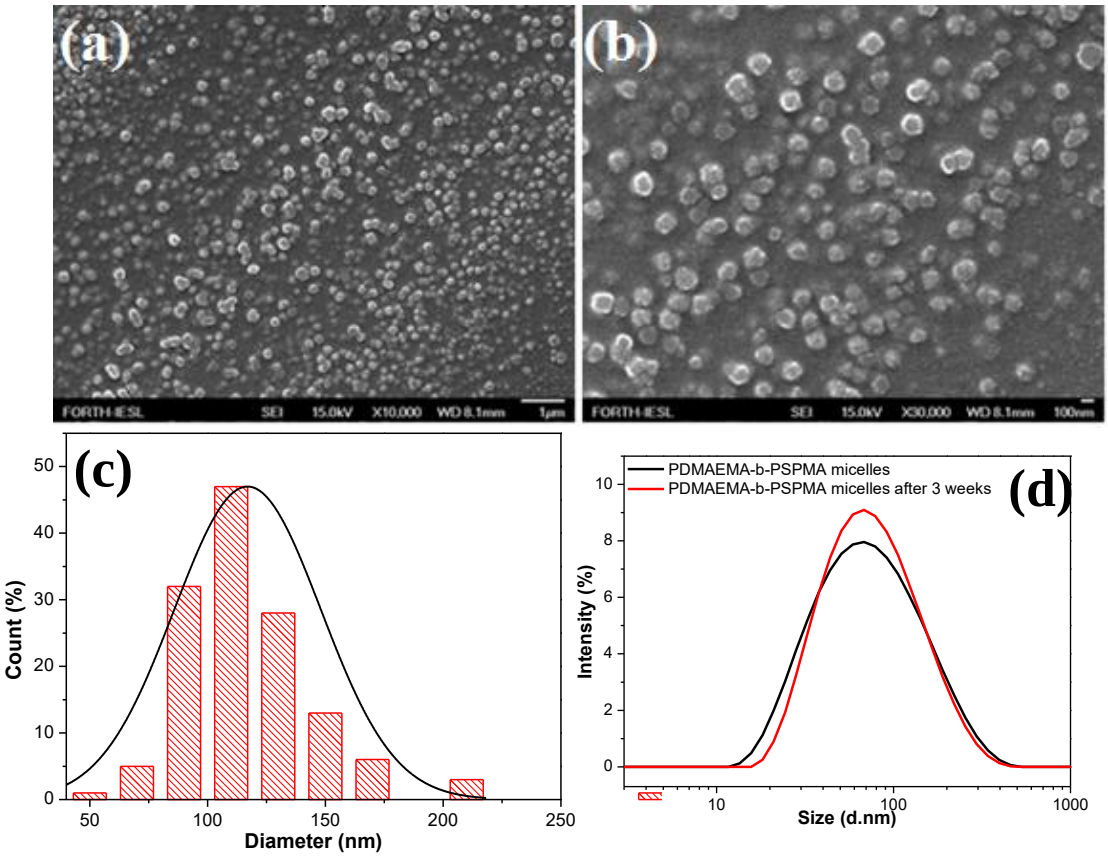

Figure 30: (a, b) FESEM images of the PDMAEMA-*b*-PSPMA diblock copolymer micelles formed in aqueous solution, (c) size distribution of the micelles by FESEM and (d) DLS measurements of the copolymer micelles at t = 0 (black line) and after 3 weeks in solution (red line).

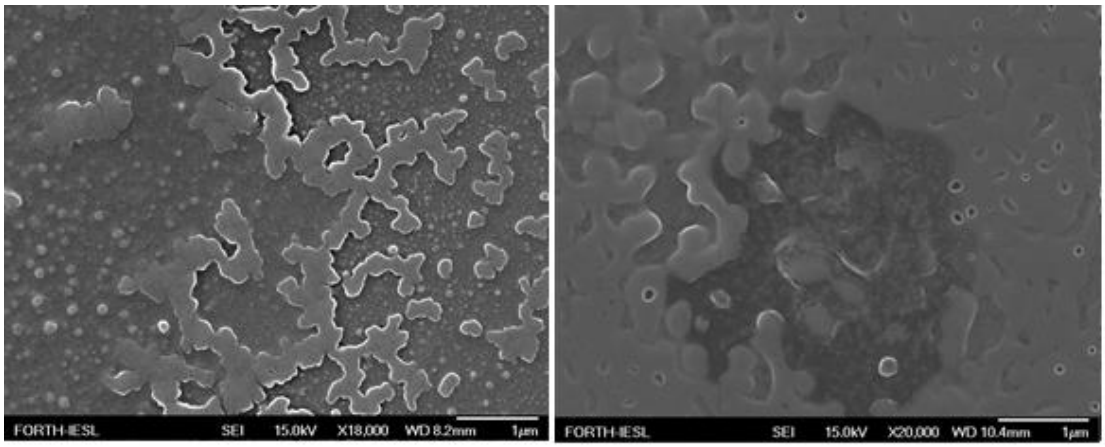

Figure 31: FESEM images of the PDMAEMA-*b*-PSPMA diblock copolymer after irradiation with UV light for 25 min.

Furthermore, the UV irradiated sample was irradiated with visible light for 2.5 h to induce the isomerization of MC back to the SP form. During the irradiation the colour of the solution changed from light purple to colourless-yellowish indicating the ring-closure isomerization of the MC species. After visible light irradiation, a drop of the sample was deposited on the silicon wafer and was dried overnight at room temperature, before being measured by FESEM. The FESEM images revealed the reformation of spherical nanostructures, with significantly larger size compared to the initial micelles (D = 213 ± 36 nm), whereas some patches of a remaining film were also observed, suggesting that the isomerization of MC-to-SP was not complete, or that the reformation of the spherical structures was hindered (**Figure 32**).

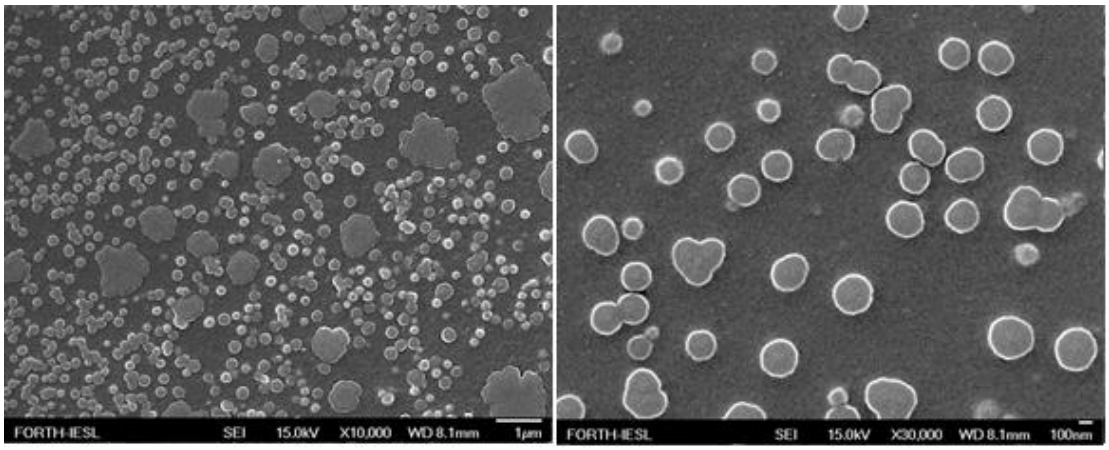

Figure 32: FESEM images of the PDMAEMA-*b*-PSPMA diblock copolymer after sequential irradiation with UV light (25 min) and visible light (2.5 h).

Further observation of the UV irradiated sample after 2 days (**Figures 33a-c**) and 4 days (**Figures 33d-f**), revealed the formation of rod-like particles, whose length increased with time. The length of these unique structures after 2 days was ~1 μm, while after 4 days it increased significantly to 6.3 ± 0.7 μm. Moreover, in both cases higher magnification images showed that these elongated particles consisted of multiple rod-like particles in a liquid-crystalline type of assembly.

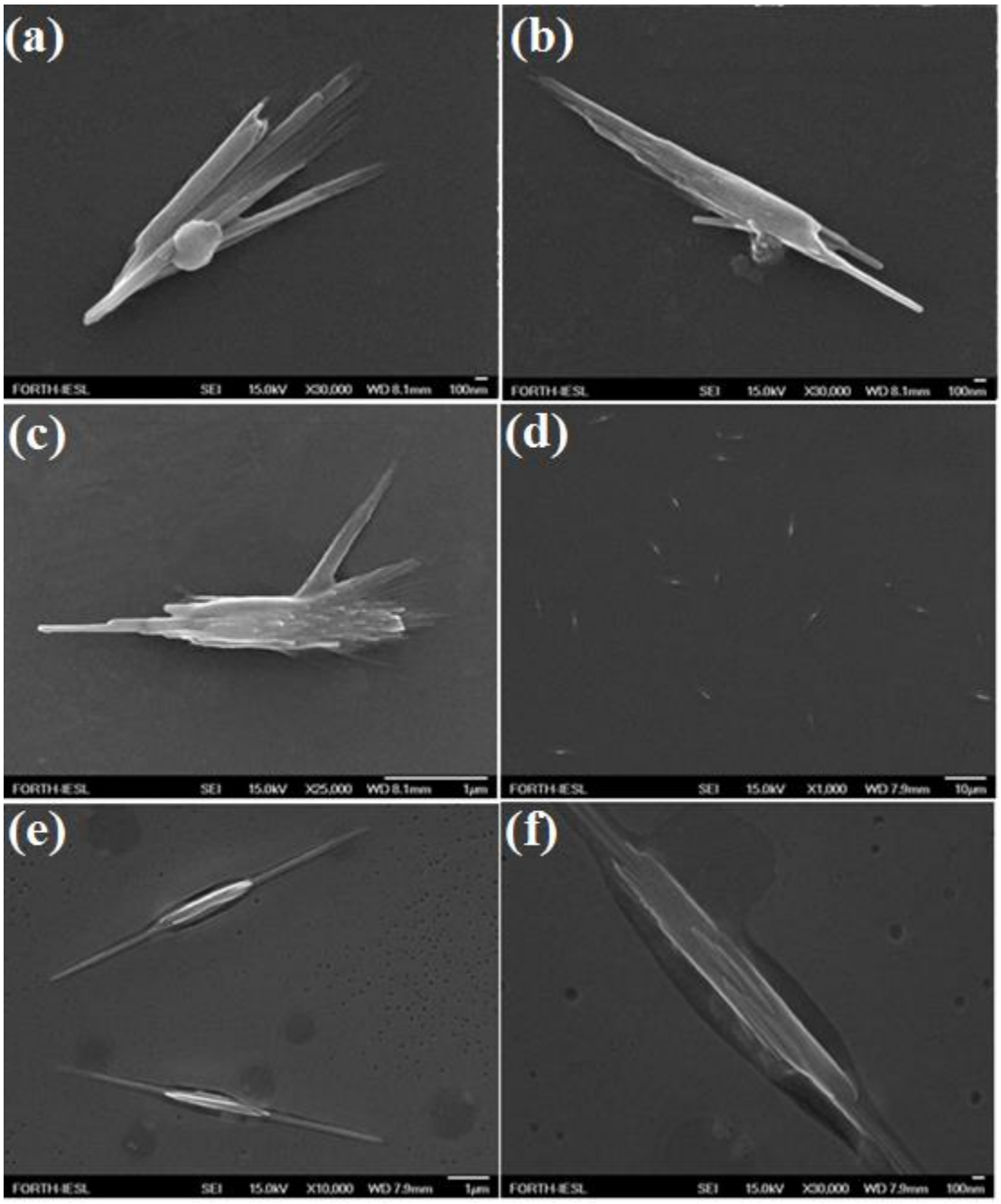

Figure 33: FESEM images of the UV-irradiated PDMAEMA-*b*-PSPMA diblock copolymer after 2 days (a-c) and 4 days (d-f) in solution.

The prolonged monitoring of the sample after 7 days in solution revealed the disappearance of the rods and the formation of extremely long (~100 μm) and intertwined helical ribbons **(Figure 34)**. Higher magnification images of the left-handed ribbons showed that their terminus consisted of many separate interwoven fibers self-assembled to form the hierarchical superstructures (**Figure 34b**).

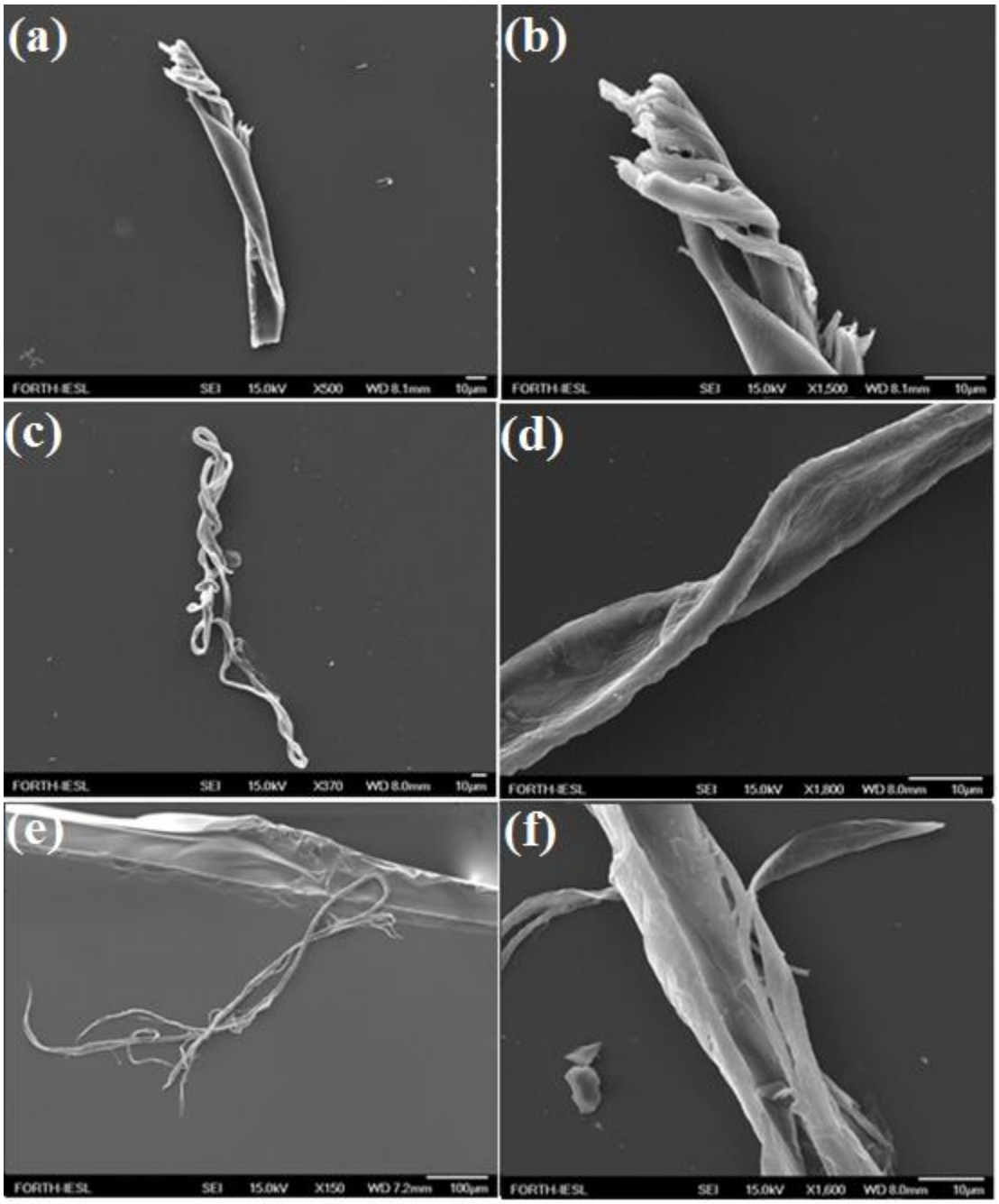

Figure 34: FESEM images of the UV-irradiated PDMAEMA-*b*-PSPMA diblock copolymer after 7 days in solution.

Morphological changes of the spiropyran-based self-assembled structures upon UV irradiation or under acidic conditions have been reported previously, manifesting the role of the merocyanine moieties in these unique self-assembly behavior of the systems.[41,65] These unusual self-assemblies are attributed to the interactions between the MC isomers, including dipole-dipole, π-π stacking between the aromatic rings as well as hydrogen bonding interactions. The first report on these unique properties of MC, described the formation of MC supramolecular aggregates in nonpolar solvents under UV irradiation and in the presence of a constant electric field.[66] The quasi crystals formed comprised globules that were linked together and aligned along the electric force. In addition, the spontaneous formation of highly organized spiropyran-based microcrystalline structures at the liquid/air interface has been reported.[67] Recently the tunable morphological change of a spiropyran molecule from nanospheres to nanorods, assisted by an acid stimulus, was reported and attributed to the π-π stacking and hydrogen bonding of the MC moieties.[65] However, the self-assemblies formed by the diblock copolymers prepared in this work, after UV irradiation of the sample, are distinct and differ from the aggregates described above. The synthesized spiropyran-based copolymers displayed a high degree of organization and uniform morphologies from the nano to the micro scale. In addition, these assemblies were characterized by high complexity and adjustable morphology with time. The driving forces that transformed the structure-less polymer (upon UV irradiation) to the rod-like particles and then sequential to their organization into the long interwind helical ribbons are hypothesized to be the intermolecular forces between the MC isomers, dipole-dipole, π-π stacking between the aromatic rings and hydrogen bonding interactions with the surrounding water molecules, however, the dynamics and the kinetics of this self-assembly process are still unclear and are under further investigation in our lab.

3.6 Synthesis of the PEG-*b*-PDMAEMA-*b*-PSPMA triblock copolymer

3.6.1 Synthesis of the macromolecular CTA, $mPEG_{113}$-CDTPA (macro-CTA)

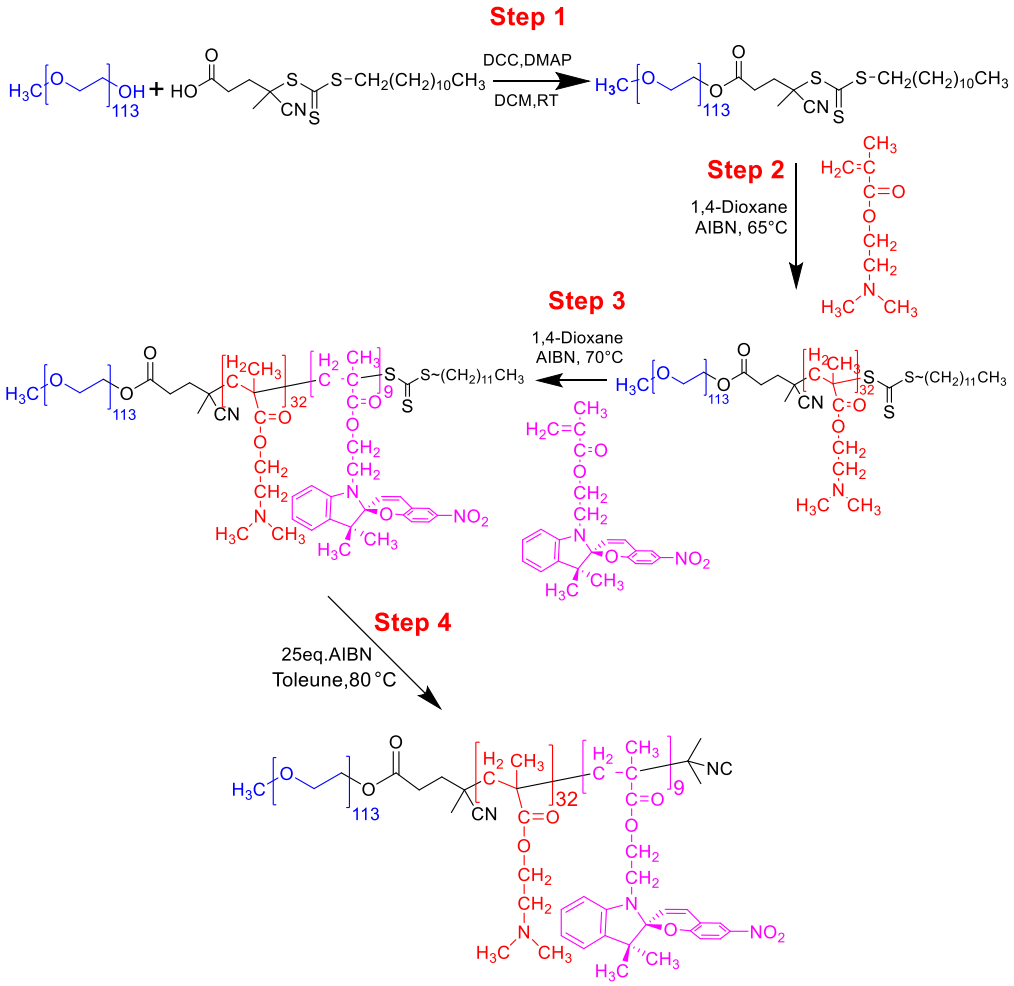

Figure 35: Synthetic route employed for the preparation of the PEG-*b*-PDMAEMA-*b*-PSPMA triblock copolymers.

Following a similar procedure to that described above for the preparation of the diblock copolymer, a triblock copolymer was also synthesized via radical addition-fragmentation chain transfer polymerization (RAFT) (**Figure 35**). First, the PEG macro-CTA was synthesized by a typical esterification reaction using 4-cyano-4-[(dodecylsulfanylthiocarbonyl)sulfanyl] pentanoic acid as the CTA in dry dichloromethane in the presence of DCC, catalyzed by DMAP (**Figure 35, Step 1**). The successful synthesis of the macro-CTA was verified by SEC. From the

monomodal and narrow SEC curve (**Figure 36, black line**) the resulting number average molecular weight and molecular weight distribution of $mPEG_{113}$-CDTPA were found M_n = 14300 g/mol and M_w/M_n = 1.04, respectively. Surprisingly, SEC analysis gave us systematically higher molecular weights compared to the nominal values, and therefore, NMR analysis was used to determine the molecular weight of the polymers, instead. First, the successful synthesis of the macro-CTA was verified by ^{1}H NMR spectroscopy (**Figure 37**). The ^{1}H NMR spectrum of the polymer exhibited peaks attributed to both $mPEG_{113}$ and the CDTPA. The appearance of two new signals at 4.24-4.28 ppm and 3.76-3.80 ppm, assigned to the methylene protons of mPEG, next to the newly formed ester bond, confirmed the successful synthesis of $mPEG_{113}$-CDTPA. In addition, the molecular weight of PEG was calculated by ratioing the peak integrals of the methyl protons of mPEG at 3.4 pmm (H-k) over the methylene protons of the PEG repeat unit at 3.62 ppm (H-j) and was found M_n = 4900 g/mol.

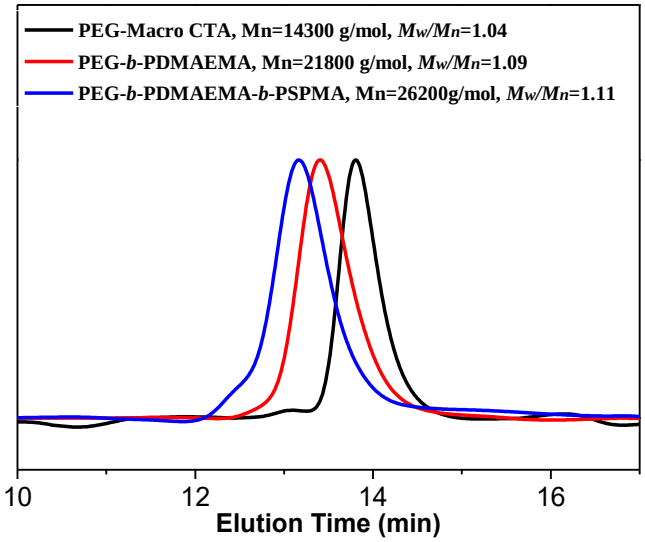

Figure 36: SEC traces of the PEG macro-CTA (black line), the diblock copolymer PEG-*b*-PDMAEMA macro-CTA (red line) and the PEG-*b*-PDMAEMA-*b*-PSPMA triblock copolymer (blue line).

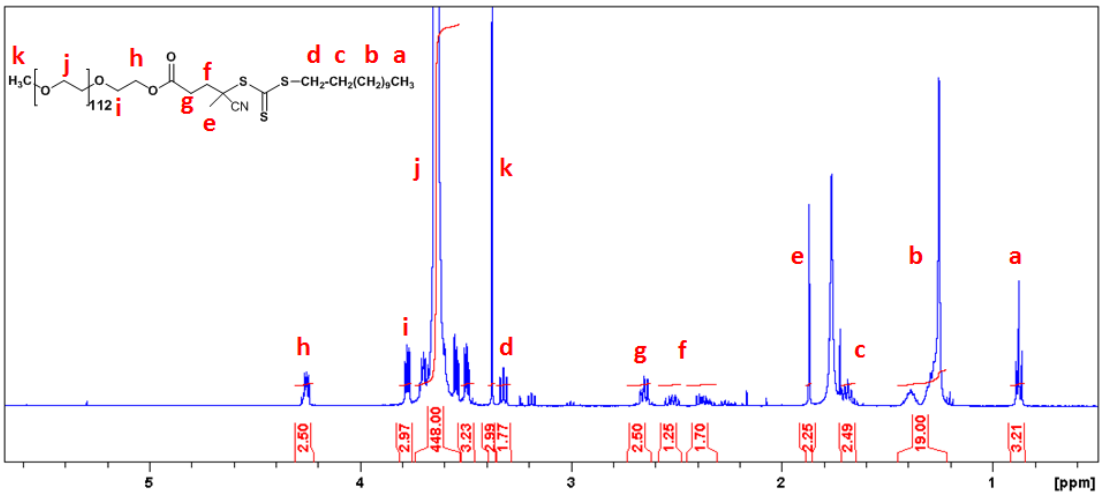

Figure 37: ^{1}H NMR spectrum of mPEG$_{113}$-CDTPA in $CDCl_3$

3.6.2 Synthesis of the diblock copolymer PEG$_{113}$-*b*-PDMAEMA$_x$ macro-CTA

The synthesized PEG$_{113}$-CDTPA macroinitiator was next employed for the polymerization of DMAEMA, using AIBN as the initiator in 1,4-dioxane at 65 °C for 28 h (**Figure 35, Step 2**). The successful polymerization was verified by SEC and ^{1}H NMR spectroscopy. The monomodal SEC curve (**Figure 36, red line**) shifted towards lower elution times, without any traces of the PEG$_{113}$-CDTPA macroinitiator, indicating the controlled growth of the polymer chains as well as the living character of the polymerization. The resulting number average molecular weight and molecular weight distribution of the PEG$_{113}$-*b*-PDMAEMA diblock copolymer were found M_n = 21800 g/mol and M_w/M_n = 1.09, respectively again much higher than the expected molecular weight. On the other hand, the ^{1}H NMR spectrum of the product exhibited peaks attributed to both the PEG and PDMAEMA blocks, and allowed to determine the chemical composition of the diblock polymer (**Figure 38)**. The mole ratio between the two blocks, PEG and PDMAEMA, was determined by comparing the peak integrals of the signal at 3.65 ppm (O-(CH_2)$_2$, H-k) attributed to the PEG block and the signal at 2.56 ppm (CH_2-N, H-w) due to the PDMAEMA block. Taking into account the M_n of the PEG block, which corresponds to 113 repeat units, the degree of polymerization of the PDMAEMA block was found 32, which corresponds to an M_n = 5000 g/mol.

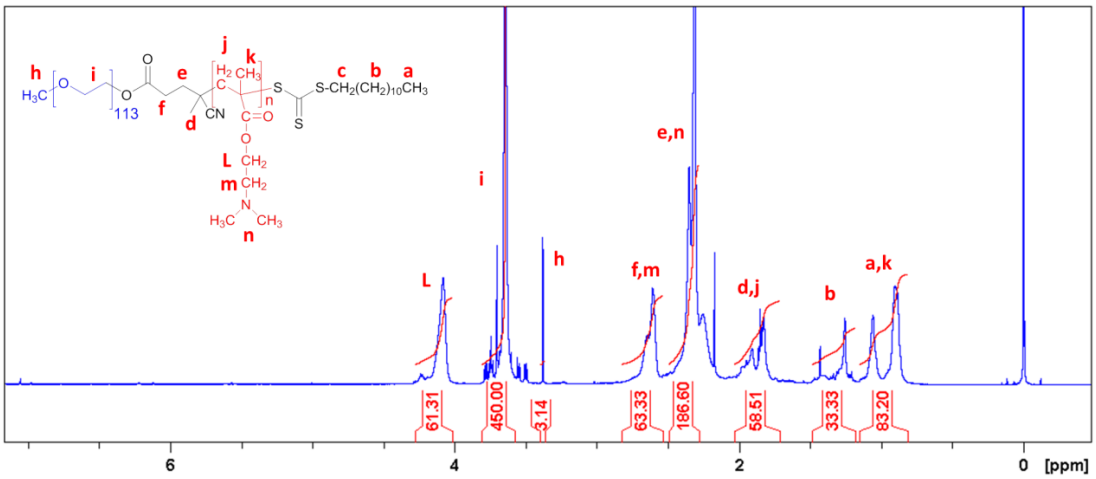

Figure 38: ^{1}H NMR spectrum of mPEG$_{113}$-*b*-PDMAEMA in $CDCl_3$

3.6.3 Synthesis of the PEG-*b*-PDMAEMA-*b*-PSPMA triblock copolymer

Finally, the synthesized PEG$_{113}$-*b*-PDMAEMA$_{32}$ macroinitiator was used for the polymerization of SPMA to prepare the PEG-*b*-PDMAEMA-*b*-PSPMA triblock copolymer (**Figure 35, Step 3**). The successful polymerization was again verified by SEC and ^{1}H NMR spectroscopy. The monomodal SEC curve (**Figure 36, blue line**) shifted towards lower elution times, without any traces of the PEG$_{113}$-*b*-PDMAEMA macroinitiator, indicating the controlled growth of the polymer chains as well as the living character of the polymerization. The resulting number average molecular weight and molecular weight distribution of the PEG-*b*-PDMAEMA-*b*-PSPMA triblock copolymer were found M_n = 26200 g/mol and M_w/M_n =1.11, respectively, consistently higher than the expected value. However, the ^{1}H NMR spectrum of the triblock copolymer (**Figure 39 bottom spectrum**) exhibited peaks attributed to all three blocks (PEG, PDMAEMA, PSPMA) and allowed to calculate the composition and the molecular weight of the copolymer. The molar ratio of the three blocks, PEG, PDMAEMA and PSPMA, was determined by ratioing the peak integrals of the signal at 7.88 ppm (Ar-*H*, H-a,b) corresponding to the PSPMA block, the signal at 2.56 ppm (C*H*$_2$-N, H-w) attributed to the PDMAEMA block and the signal at 3.65 ppm (O-(C*H*$_2$)$_2$, H-k) attributed to the PEG block. Given the degree of polymerization of the PEG and PDMAEMA blocks determined above for the diblock copolymer precursor, the DP of the PSPMA block was calculated DP = 9. Therefore, the molar ratio of the three blocks, PEG-PDMAEMA-PSPMA was found 113-32-9, which corresponds to a

PEG-PDMAEMA-PSPMA content of 73-21-6 mol% and a weight fraction of 35-37-28 wt% for the triblock copolymer. Moreover, from these data the number average molecular weight of the SPMA block was found M_n = 3800 g/mol and of the triblock copolymer M_n = 13700 g/mol.

3.6.4 End group modification of the PEG-*b*-PDMAEMA-*b*-PSPMA triblock copolymer

The end group modification of the synthesized triblock copolymer took place using an excess of AIBN in toluene at 80 °C for 3 h (**Figure 35, Step 4**). The successful reaction was verified by ^{1}H NMR spectroscopy (**Figure 39, bottom spectrum**). The integral of the peaks at 0.5-1.5 ppm, in which the methyl and methylene protons of the CDTPA appeared, decreased after the modification indicating the loss of the polymer end groups. In addition, the appearance of a new peak at 1.56 (H-p), which corresponds to the methyl protons of the AIBN fragment ((CH_3)$_2$CN) that is attached at the polymer chain end, confirms the successful polymer derivatization.

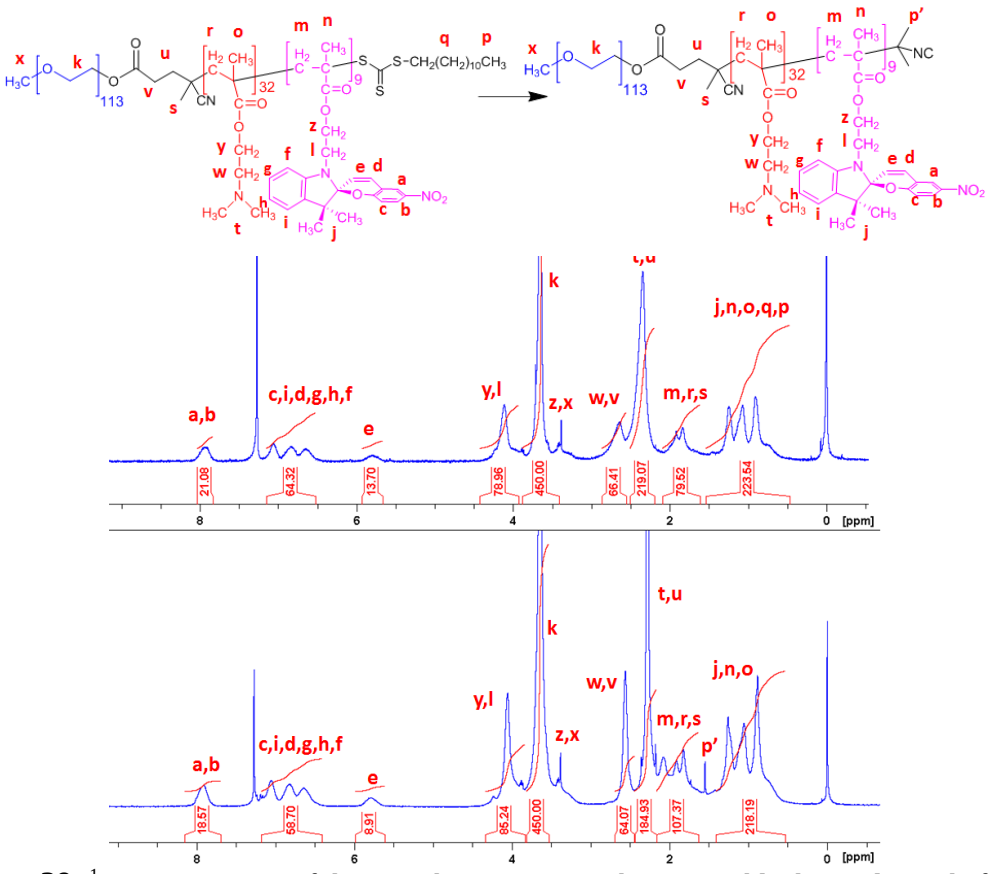

Figure 39: ^{1}H NMR spectra of the PEG-*b*-PDMAEMA-*b*-PSPMA block copolymer before (top spectrum) and after (bottom spectrum) end group modification in $CDCl_3$.

3.7 Photo-responsive properties of the PEG-*b*-PDMAEMA-*b*-PSPMA triblock copolymer in aqueous media

The photo-responsive behavior of the PEG-*b*-PDMAEMA-*b*-PSPMA triblock copolymer in aqueous media was monitored by UV/Vis spectroscopy. The absorption spectra of the triblock copolymer as a function of irradiation time, with UV light at λ = 365 nm, are shown in **Figure 40**. Before UV irradiation, the absorption at λ > 450 nm is relatively low, suggesting that the SPMA units are in their spiropyran form. Following irradiation with UV light, the ring-opening isomerization of SP to MC was confirmed by the constant increase of the intensity of the absorption band from 450 to 650 nm. The maximum isomerization of SP to MC was achieved after 20 min of UV irradiation, and was accompanied by a spontaneous change of the color of the sample, from colorless to purple, confirming the formation of the conjugates MC isomer. Furthermore, an increase of the absorption intensity in the 370 nm - 440 nm range was detected, which was assigned to the open non-planar X isomer. It is noted again that the absorption maximum of the merocyanine was red-shifted, from 577 nm to 561 nm, as a function of irradiation time, indicating the formation of as discussed above for the PDMAEMA-*b*-PSMA diblock copolymer (**Section 3.4**).

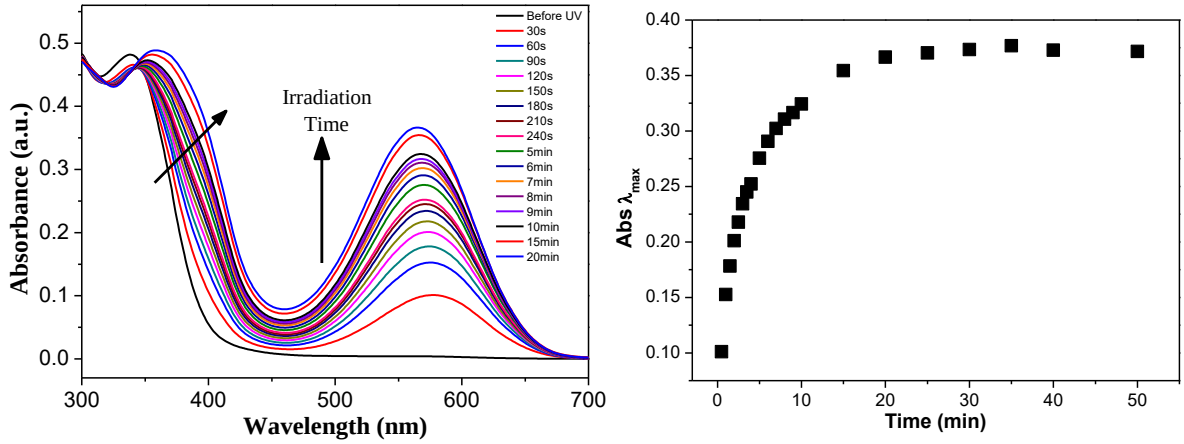

Figure 40: **Left:** UV/Vis absorption spectra of an aqueous PEG-*b*-PDMAEMA-*b*-PSPMA copolymer solution upon UV irradiation. **Right:** Increase of the absorption intensity of MC, at λ_{max}, as a function of irradiation time.

Next, the UV irradiated sample (20 min) was used to conduct a kinetic study of the isomerization of MC back to the SP form, upon visible light irradiation. **Figure 41** shows the time-dependent change in the absorption spectra of the triblock copolymer as a function of irradiation with visible light. The absorption band of MC (450 nm - 650 nm) gradually decreased, however even after 90 min of irradiation with visible light a notable absorption was observed, as discussed above for the diblock copolymer, and suggested that the MC-to-SP isomerization is not quantitative. It is noted that, the MC isomer does not fully reverse back to the SP form even after prolonged irradiation, and the system reaches the so-called photostationary state.[38] Moreover, as the absorption intensity of the merocyanine isomer gradually decreased, a slight blue shift of the MC absorption band, from 565 to 570 nm was detected. In parallel a decrease of the absorption intensity of the non-planar isomer X (370 nm - 440 nm) was found, verifying the reversibility of the photo-induced process.

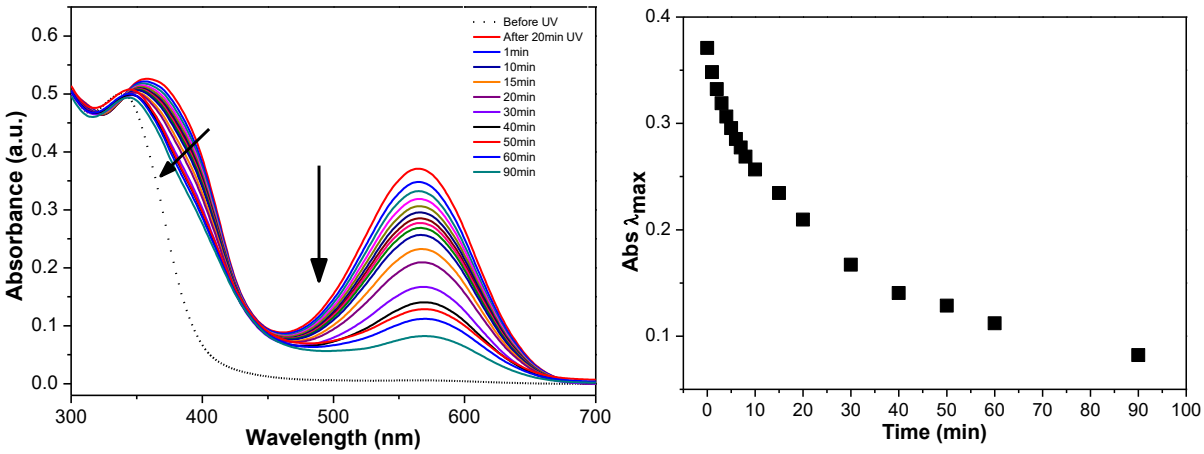

Figure 41: **Left:** UV/Vis absorption spectra of an aqueous PEG-*b*-PDMAEMA-*b*-PSPMA copolymer solution upon visible light irradiation. **Right:** Decrease of the absorption intensity of MC, at λ_{max}, as a function of irradiation time.

A kinetic study of the thermal isomerization of MC to SP was also conducted following the decrease of the intensity of the MC peak of the UV irradiated sample at 37 °C for 2.5 h. **Figure 42** (**left**) shows the time-dependent change of the absorption spectra of the triblock copolymer at 37 °C. The absorption band of the MC isomer diminishes rapidly in the first 5 min, but afterwards the decrease slows down and becomes gradual with time. After 2.5 h at 37 °C, the merocyanine does not fully reverse back to the closed spiropyran isomer with the system reaching a photostationary state. It is also noted that the thermal relaxation of MC (**Figure 42, right**) is slower compared to the light induced process discussed above (**Figure 41, right**), signifying the contribution of the light stimulus. Moreover, the thermal-induced MC-to-SP isomerization is slower in aqueous compared to organic media, which is attributed to the polar nature of MC, leading to stronger interactions with the highly polar water molecules and to the stabilization of MC in water.[68,69]

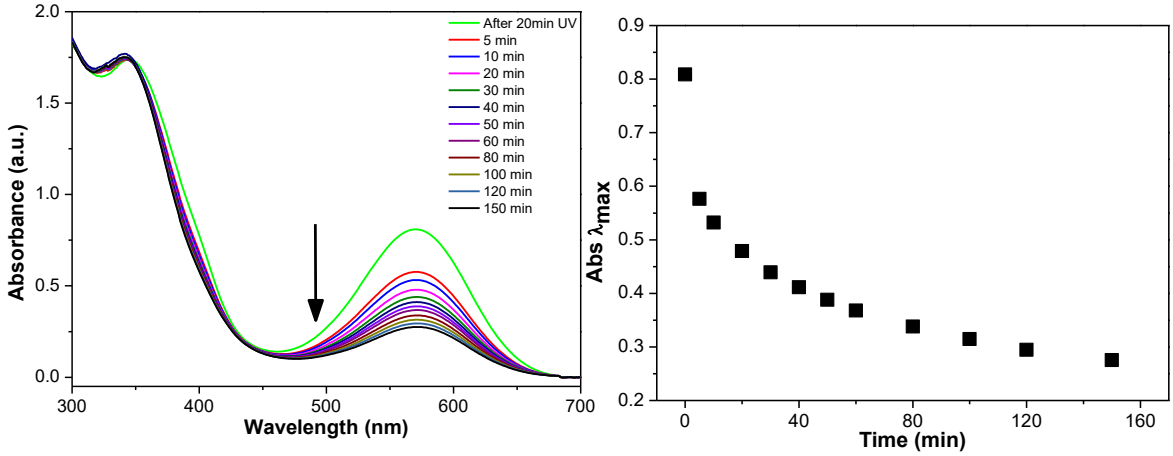

Figure 42: **Left:** UV/Vis absorption spectra of an aqueous PEG-*b*-PDMAEMA-*b*-PSPMA copolymer solution at 37 °C as a function of time. **Right:** Decrease of the absorption intensity of MC, at λ_{max}, as a function of time.

3.8 Self-assembly behavior of the PEG-*b*-PDMAEMA-*b*-PSPMA triblock copolymer in aqueous media

Having established the photo-responsive behavior of the triblock copolymer, its morphology in water was investigated. The triblock copolymer comprises a hydrophobic photo-, pH- and temperature-sensitive poly(spiropyran methacrylate) (PSPMA) block, a hydrophilic, pH- and temperature-sensitive poly(2-(dimethylamino)ethyl methacrylate)) (PDMAEMA) block and a hydrophilic poly(ethylene glycol) (PEG) block, and is thus expected to self-assemble into spherical core-shell-corona micelles in water. The influence of UV and visible light irradiation on the morphology and size of the copolymer micelles were monitored by FESEM and DLS. Following the micellization process, the polymer concentration was adjusted to c = 0.0025 wt%, and a drop of the solution was deposited on the silicon wafer and was dried overnight at room temperature for use in FESEM. The FESEM images revealed spherical micelles with a diameter D = 53 ± 14 nm and relatively uniform size distribution (**Figure 43**).

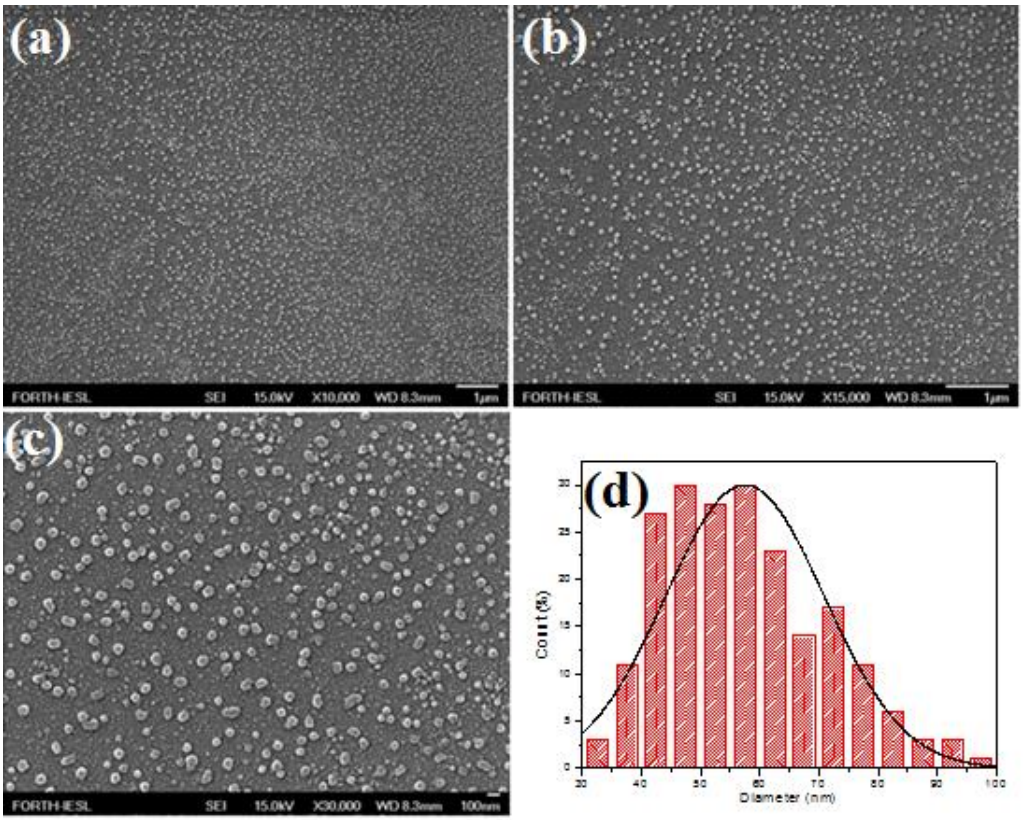

Figure 43: FESEM images of the triblock copolymer micelles formed in aqueous solution (a-c) and size distribution of the copolymer micelles by FESEM (d).

The size and the stability of the micelles were also examined using dynamic light scattering (**Figure 44**). The average hydrodynamic diameter of the triblock copolymer micelles was found D_h = 40 nm, in good agreement with the FESEM results discussed above. To investigate the stability of the micelles in water, a sample of the copolymer micelles was analyzed again by DLS 3 weeks after its preparation and the hydrodynamic diameter was found identical to the initial size, proving the excellent stability of the nanostructures.

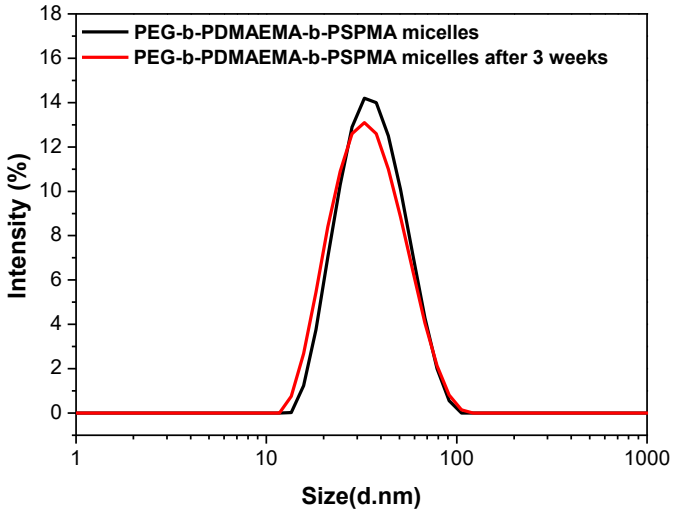

Figure 44: DLS measurements of the triblock copolymer micelles at t = 0 (black line) and after 3 weeks in solution (red line).

Next, the micellar copolymer solution was placed in a quartz cuvette and was irradiated with UV light for 20 min prior to FESEM observation. After the irradiation with UV light the sample showed the formation of a film with shapeless structures (**Figure 45**), which were attributed to the disintegration of the copolymer micelles upon isomerization of the hydrophobic spiropyran to the hydrophilic merocyanine moieties.

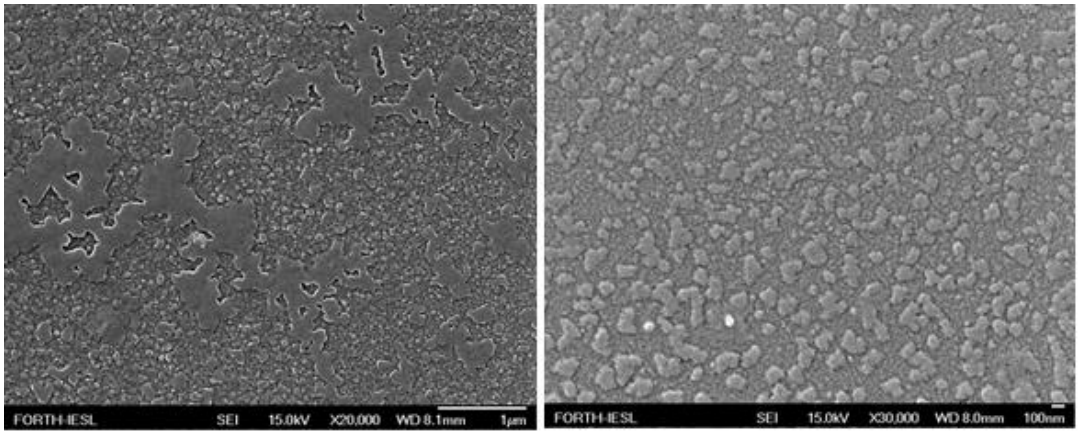

Figure 45: FESEM images of the PEG-*b*-PDMAEMA-*b*-PSPMA triblock copolymer after irradiation with UV light for 20 min.

Afterwards, the UV irradiated sample was further irradiated with visible light for 2.5 h. During irradiation the colour of the solution changed from light purple to colourless-yellowish, signifying the isomerization of MC back to the SP units. The sample was next deposited on a silicon wafer and was dried for FESEM observation. The FESEM images revealed the reformation of spherical copolymer nanostructures (**Figure 46**), but of a significantly larger size, D = 180 ± 40 nm, compared to the initially formed micelles, which suggest the structural reorganization of the copolymer chains to form larger or looser structures, similar to results discussed above for the PDMAEMA-b-PSPMA diblock copolymer (**Section 3.5**). This increase in size could be either attributed to water swollen polymer micelles, due to the remaining hydrophilicity of the PSPMA block, which reaches the photostationary state, and/or to the organization of the copolymer chains into polymer vesicles. The elucidation of the precise morphology of these polymer nanostructures will be examined as part of the future work on these systems.

Further observation of the UV irradiated sample after 3 days revealed again the formation of rod-like particles, with length ~1 ± 0.2 μm and width ~212 ± 51 nm, as shown in **Figure 47**. These structures are morphological similar to those obtained for the PDMAEMA-*b*-PSPMA diblock copolymer after being kept for 2 and 4 days in solution.

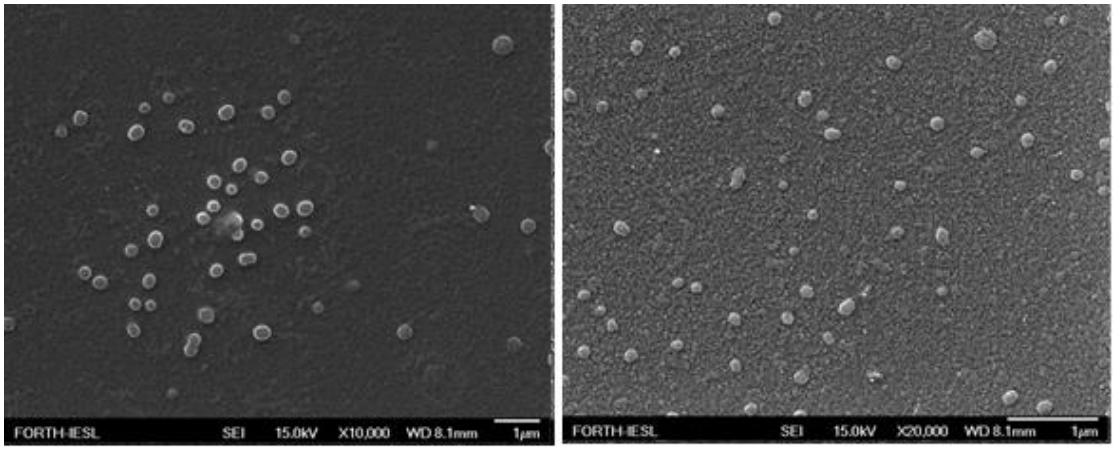

Figure 46: FESEM images of the PEG-*b*-PDMAEMA-*b*-PSPMA triblock copolymer after sequential irradiation with UV (20 mins) and visible (2.5 h) light.

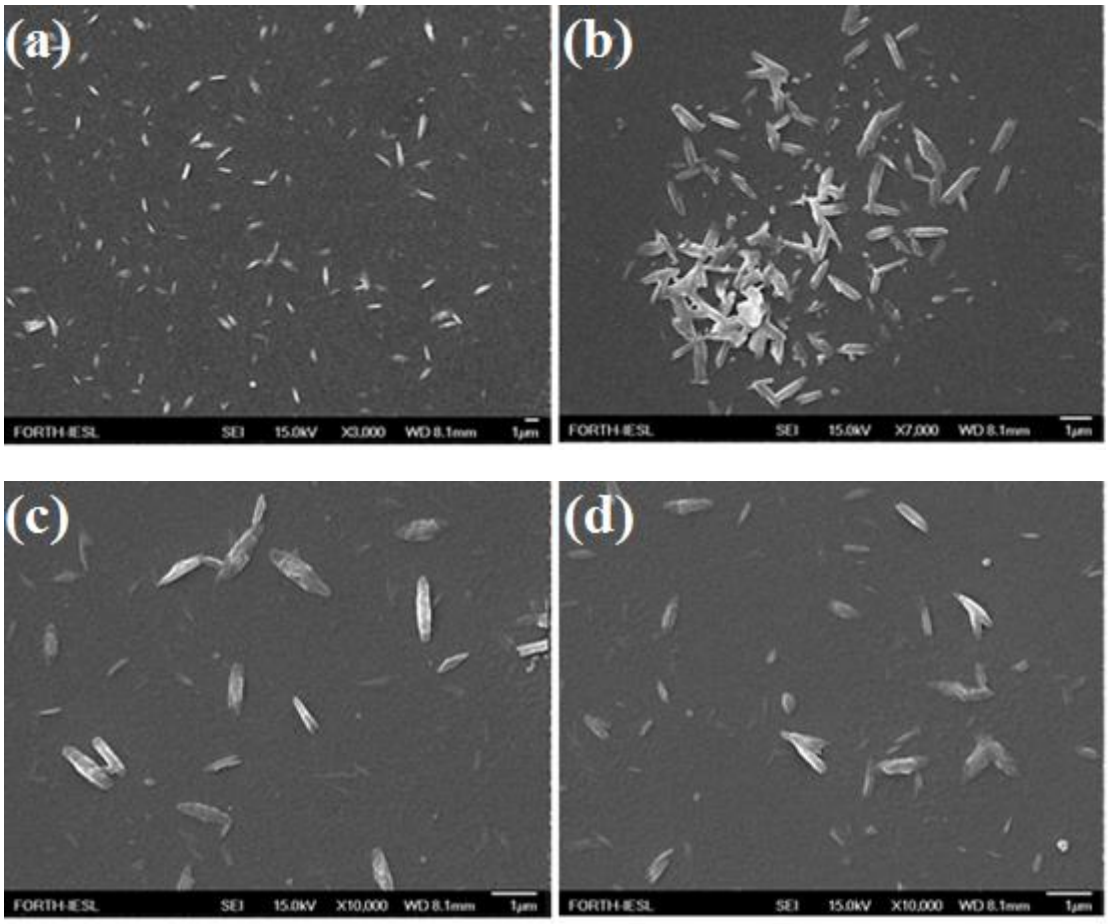

Figure 47: FESEM images of the UV-irradiated PEG-*b*-PDMAEMA-*b*-PSPMA triblock copolymer after 3 days in solution.

And finally, as expected, extended monitoring of the sample after 7 days in solution revealed the disappearance of the rods and the formation of extremely long (100's μm) and complex helical ribbons (**Figure 48**). Higher magnification images of the ribbons revealed that the terminus of these left-handed superstructures comprised many individual fibers that interlaced to form the hierarchical assemblies (**Figure 48c, d and h**).

These results are identical to those obtained for the diblock copolymers discussed above, and are very interesting, suggesting that the MC stacking could be a very powerful and generic tool for the hierarchical self-assembly of these SPMA-based block copolymers leading to the design of unique and very complex superstructures. Further studies are underway to elucidate the structure of these assemblies as well as the kinetics of the self-assembly process.

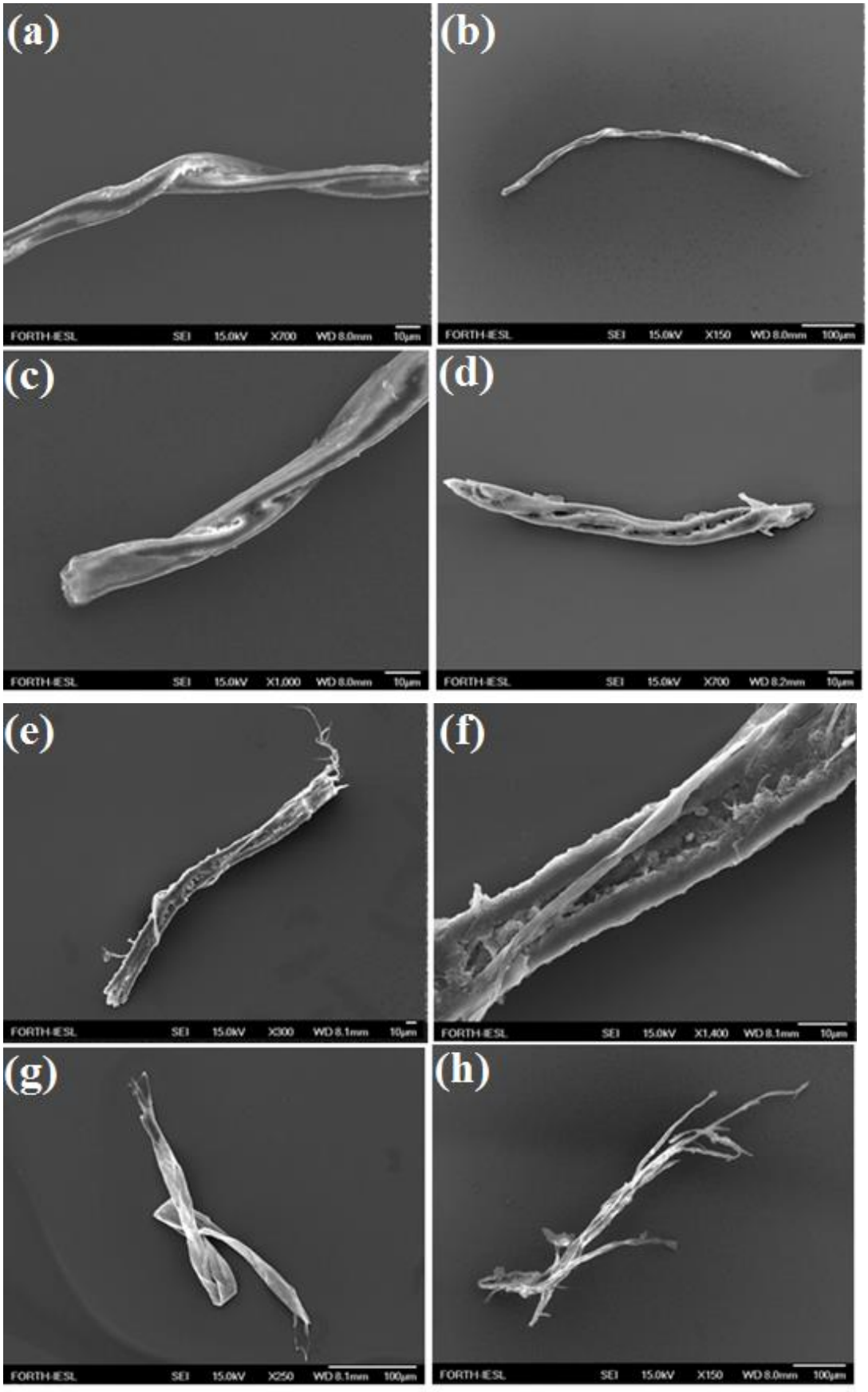

Figure 48: FESEM images of the UV-irradiated PEG-*b*-PDMAEMA-*b*-PSPMA triblock copolymer after being kept for 7 days in solution.

4. Conclusions and Future Perspectives

In this work, multi-responsive amphiphilic triblock and diblock copolymers, based on SPMA, were synthesized via RAFT polymerization. The novel triblock copolymer consisted of a hydrophobic, temperature-, pH- and light-responsive PSPMA block, a hydrophilic, temperature- and pH-responsive PDMAEMA block and a neutral, hydrophilic PEG block, while the diblock copolymer comprised a PDMAEMA and a PSPMA block. The PEG-*b*-PDMAEMA-*b*-PSPMA triblock copolymer self-assembled into well-defined and stable spherical core-shell-corona micelles in water, whereas the PDMAEMA-*b*-PSPMA diblock copolymer formed spherical core-shell micelles under the same conditions. The response and the morphological behavior of the copolymer micelles, following UV and visible light irradiation, were studied by UV/vis spectroscopy, FESEM and DLS. In particular, the disassembly of the micelles after exposure to UV light, and the copolymer re-assembly into large nanostructures, following sequential irradiation with visible light, was evidenced by FESEM for both the diblock and triblock copolymers. Further analysis of the UV-irradiated copolymers revealed the formation of large rod-like particles (a few μm long) at earlier times (2-4 days after irradiation) and the presence of very long (100's μm) helical ribbon-like superstructures at longer times (7 days after irradiation). It is believed that these self-assemblies, which are characterized by high morphological complexity, were obtained due to the MC-MC, MC-SP and MC-water interactions (dipole-dipole interactions, π-π stacking and hydrogen bonding) in the sample. The detailed investigation of the polymorphism that these spiropyran-based polymers has presented is still ongoing and could be part of the future work on these systems.

In the second part of this thesis, a bifunctional spiropyran molecule has been successfully synthesized. This spiropyran bears two hydroxyl functional groups and

can be used, after one more modification step to transform the alcohol to a bromide, as a cross-linker to form shell cross-linked core-shell-corona micelles. For example, when combined with the PEG-*b*-PDMAEMA-*b*-PSPMA triblock copolymer micelles prepared in this work, it could lead to the quaternization of the PDMAEMA shell to give pH-, temperature-, light and mechano-responsive micelles. This would be a pioneering system for in depth investigation in the future, since there is no report in the literature so far on such multi-responsive micellar systems.

5. References

1. Wei, M., Gao, Y., Li, X. & Serpe, M. J. Stimuli-responsive polymers and their applications. *Polym. Chem.* **8**, 127–143 (2017).
2. Stuart, M. A. C. *et al.* Emerging applications of stimuli-responsive polymer materials. *Nature Mater* **9**, 101–113 (2010).
3. Heskins, M. & Guillet, J. E. Solution Properties of Poly(N-isopropylacrylamide). *Journal of Macromolecular Science: Part A - Chemistry* **2**, 1441–1455 (1968).
4. Liu, R., Fraylich, M. & Saunders, B. R. Thermoresponsive copolymers: from fundamental studies to applications. *Colloid Polym Sci* **287**, 627–643 (2009).
5. Hoogenboom, R. Temperature-responsive polymers: properties, synthesis and applications. in *Smart Polymers and their Applications* 15–44 (Elsevier, 2014). doi:10.1533/9780857097026.1.15.
6. Manouras, T. & Vamvakaki, M. Field responsive materials: photo-, electro-, magnetic- and ultrasound-sensitive polymers. *Polym. Chem.* **8**, 74–96 (2017).
7. Dai, S., Ravi, P. & Tam, K. C. pH-Responsive polymers: synthesis, properties and applications. *Soft Matter* **4**, 435 (2008).
8. Baines, F. L., Billingham, N. C. & Armes, S. P. Synthesis and Solution Properties of Water-Soluble Hydrophilic−Hydrophobic Block Copolymers. *Macromolecules* **29**, 3416–3420 (1996).
9. Gillies, E. R. & Fréchet, J. M. J. pH-Responsive Copolymer Assemblies for Controlled Release of Doxorubicin. *Bioconjugate Chem.* **16**, 361–368 (2005).
10. Thévenot, J., Oliveira, H., Sandre, O. & Lecommandoux, S. Magnetic responsive polymer composite materials. *Chem. Soc. Rev.* **42**, 7099 (2013).
11. Palza, H., Zapata, P. & Angulo-Pineda, C. Electroactive Smart Polymers for Biomedical Applications. *Materials* **12**, 277 (2019).

12. Irie, M. Properties and applications of photoresponsive polymers. *Pure and Applied Chemistry* **62**, 1495–1502 (1990).
13. Wang, X. *et al.* Reversibly Switching Bilayer Permeability and Release Modules of Photochromic Polymersomes Stabilized by Cooperative Noncovalent Interactions. *J. Am. Chem. Soc.* **137**, 15262–15275 (2015).
14. Jochum, F. D. & Theato, P. Temperature- and light-responsive smart polymer materials. *Chem. Soc. Rev.* **42**, 7468–7483 (2013).
15. Wang, D., Green, M. D., Chen, K., Daengngam, C. & Kotsuchibashi, Y. Stimuli-Responsive Polymers: Design, Synthesis, Characterization, and Applications. *International Journal of Polymer Science* **2016**, 1–2 (2016).
16. Zhang, J., Li, X. & Li, X. Stimuli-triggered structural engineering of synthetic and biological polymeric assemblies. *Progress in Polymer Science* **37**, 1130–1176 (2012).
17. Sun, X., Agate, S., Salem, K. S., Lucia, L. & Pal, L. Hydrogel-Based Sensor Networks: Compositions, Properties, and Applications—A Review. *ACS Appl. Bio Mater.* **4**, 140–162 (2021).
18. Kotsuchibashi, Y. Recent advances in multi-temperature-responsive polymeric materials. *Polym J* **52**, 681–689 (2020).
19. Jain, K., Vedarajan, R., Watanabe, M., Ishikiriyama, M. & Matsumi, N. Tunable LCST behavior of poly(N-isopropylacrylamide/ionic liquid) copolymers. *Polym. Chem.* **6**, 6819–6825 (2015).
20. Agarwal, S., Zhang, Y., Maji, S. & Greiner, A. PDMAEMA based gene delivery materials. *Materials Today* **15**, 388–393 (2012).

21. Bütün, V., Billingham, N. C. & Armes, S. P. Synthesis and aqueous solution properties of novel hydrophilic–hydrophilic block copolymers based on tertiary amine methacrylates. *Chem. Commun.* 671–672 (1997) doi:10.1039/a700772h.
22. Verezhnikov, V. N., Plaksitskaya, T. V. & Poyarkova, T. N. pH-thermosensitive behavior of N,N-dimethylaminoethyl methacrylate (Co)polymers with N-vinylcaprolactam. *Polym. Sci. Ser. A* **48**, 870–874 (2006).
23. Kocak, G., Tuncer, C. & Bütün, V. pH-Responsive polymers. *Polym. Chem.* **8**, 144–176 (2017).
24. Reyes-Ortega, F. pH-responsive polymers: properties, synthesis and applications. in *Smart Polymers and their Applications* 45–92 (Elsevier, 2014). doi:10.1533/9780857097026.1.45.
25. Bertrand, O. & Gohy, J.-F. Photo-responsive polymers: synthesis and applications. *Polym. Chem.* **8**, 52–73 (2017).
26. Harnoy, A. J., Slor, G., Tirosh, E. & Amir, R. J. The effect of photoisomerization on the enzymatic hydrolysis of polymeric micelles bearing photo-responsive azobenzene groups at their cores. *Org. Biomol. Chem.* **14**, 5813–5819 (2016).
27. Zhang, D. *et al.* Polyion complex micelles formed by azobenzene-based polymer with multi-responsive properties. *J Appl Polym Sci* **138**, 50580 (2021).
28. Sinawang, G., Wang, J., Wu, B., Wang, X. & He, Y. Photoswitchable aggregation-induced emission polymer containing dithienylethene and tetraphenylethene moieties. *RSC Adv.* **6**, 12647–12651 (2016).
29. Irie, M., Fukaminato, T., Matsuda, K. & Kobatake, S. Photochromism of Diarylethene Molecules and Crystals: Memories, Switches, and Actuators. *Chem. Rev.* **114**, 12174–12277 (2014).

30. Babin, J. *et al.* A New Two-Photon-Sensitive Block Copolymer Nanocarrier. *Angew. Chem. Int. Ed.* **48**, 3329–3332 (2009).
31. Roche, A. *et al.* Supramolecular block copolymers as novel UV and NIR responsive nanocarriers based on a photolabile coumarin unit. *European Polymer Journal* **126**, 109561 (2020).
32. Falireas, P. G. Triple-Responsive Block Copolymer Micelles with Synergistic pH and Temperature Response. 11.
33. Lee, H. *et al.* Light-Induced Reversible Formation of Polymeric Micelles. *Angew. Chem. Int. Ed.* **46**, 2453–2457 (2007).
34. Yuan Zhang, Mengjiao Cao, Bing Yuan, Tianying Guo, & Wangqing Zhang. RAFT synthesis and micellization of a photo-, temperature- and pH-responsive diblock copolymer based on spiropyran. *Polym. Chem.* **8**, 7325–7332 (2017).
35. Díaz-Moscoso, A. & Ballester, P. Light-responsive molecular containers. *Chem. Commun.* **53**, 4635–4652 (2017).
36. Hongyan Xia , Kang Xie and Gang Zou. Advances in Spiropyrans/Spirooxazines and Applications Based on Fluorescence Resonance Energy Transfer (FRET) with Fluorescent Materials. *Molecules* (2017) doi:doi:10.3390/molecules22122236.
37. Tian, W. & Tian, J. An insight into the solvent effect on photo-, solvato-chromism of spiropyran through the perspective of intermolecular interactions. *Dyes and Pigments* **105**, 66–74 (2014).
38. Kortekaas, L. & Browne, W. R. The evolution of spiropyran: fundamentals and progress of an extraordinarily versatile photochrome. *Chem. Soc. Rev.* **48**, 3406–3424 (2019).

39. Davis, D. A. *et al.* Force-induced activation of covalent bonds in mechanoresponsive polymeric materials. *Nature* **459**, 68–72 (2009).
40. Metelitsa, A. V., Coudret, C., Micheau, J. C. & Voloshin, N. A. Quantitative investigations of thermal and photoinduced J- and H-aggregation of hydrophobic spirooxazines in binary solvent through UV/vis spectroscopy. *RSC Adv.* **4**, 20974–20983 (2014).
41. Wismontski-Knittel, T. & Krongauz, V. Self-assembling of spiropyran polymers by zipper crystallization. *Macromolecules* **18**, 2124–2126 (1985).
42. Parthiban, A. Synthesis and Applications of Copolymers. (2014) doi:10.1002/9781118860168.
43. Kamigaito, M., Ando, T. & Sawamoto, M. Metal-Catalyzed Living Radical Polymerization. *Chem. Rev.* **101**, 3689–3746 (2001).
44. Braunecker, W. A. & Matyjaszewski, K. Controlled/living radical polymerization: Features, developments, and perspectives. *Progress in Polymer Science* **32**, 93–146 (2007).
45. Bayati, S. Mixed Block Copolymer Solutions: Self-Assembly and Interactions. (2016).
46. Whitesides, G. M. & Boncheva, M. Beyond molecules: Self-assembly of mesoscopic and macroscopic components. *Proceedings of the National Academy of Sciences* **99**, 4769–4774 (2002).
47. Whitesides, G. M. & Grzybowski, B. Self-Assembly at All Scales. *Science* **295**, 2418–2421 (2002).
48. Philp, D. & Stoddart, J. F. Self-Assembly in Natural and Unnatural Systems. *Angew. Chem. Int. Ed. Engl.* **35**, 1154–1196 (1996).

49. Lehn, J.-M. Toward Self-Organization and Complex Matter. *Science* **295**, 2400–2403 (2002).
50. Palermo, V. & Samorì, P. Molecular Self-Assembly across Multiple Length Scales. *Angew. Chem. Int. Ed.* **46**, 4428–4432 (2007).
51. Assali, M., Cid, J.-J., Fernández, I. & Khiar, N. Supramolecular Diversity through Click Chemistry: Switching from Nanomicelles to 1D-Nanotubes and Tridimensional Hydrogels. *Chem. Mater.* **25**, 4250–4261 (2013).
52. Mailänder, V. & Landfester, K. Interaction of Nanoparticles with Cells. *Biomacromolecules* **10**, 2379–2400 (2009).
53. Okesola, B. O. & Smith, D. K. Applying low-molecular weight supramolecular gelators in an environmental setting – self-assembled gels as smart materials for pollutant removal. *Chem. Soc. Rev.* **45**, 4226–4251 (2016).
54. Adam Blanazs, Steven P. Armes, Anthony J. Ryan. Self-Assembled Block Copolymer Aggregates From Micelles to Vesicles. (2009).
55. Li, C. *et al.* Self-assembly of block copolymers towards mesoporous materials for energy storage and conversion systems. *Chem. Soc. Rev.* **49**, 4681–4736 (2020).
56. Gröschel, A. H. & Müller, A. H. E. Self-assembly concepts for multicompartment nanostructures. *Nanoscale* **7**, 11841–11876 (2015).
57. Li, L., Sun, R. & Zheng, R. Tunable morphology and functionality of multicomponent self-assembly: A review. *Materials & Design* **197**, 109209 (2021).
58. Jones, M.-C. & Leroux, J.-C. Polymeric micelles – a new generation of colloidal drug carriers. *European Journal of Pharmaceutics and Biopharmaceutics* **48**, 101–111 (1999).

59. Bastakoti, B. P. Chapter 10 - Multifunctional polymeric micelles as therapeutic nanostructures: targeting, imaging, and triggered release. 23.
60. Bastakoti, B. P. *et al.* Multifunctional Core-Shell-Corona-Type Polymeric Micelles for Anticancer Drug-Delivery and Imaging. *Chem. Eur. J.* **19**, 4812–4817 (2013).
61. Perrier, S. *50th Anniversary Perspective* : RAFT Polymerization—A User Guide. *Macromolecules* **50**, 7433–7447 (2017).
62. Moad, G., Rizzardo, E. & Thang, S. H. Radical addition–fragmentation chemistry in polymer synthesis. *Polymer* **49**, 1079–1131 (2008).
63. Raymo, F. M. & Giordani, S. Signal Processing at the Molecular Level. *J. Am. Chem. Soc.* **123**, 4651–4652 (2001).
64. O'Bryan, G., Wong, B. M. & McElhanon, J. R. Stress Sensing in Polycaprolactone Films via an Embedded Photochromic Compound. *ACS Appl. Mater. Interfaces* **2**, 1594–1600 (2010).
65. Wu, Z. *et al.* Tunable Morphology of Spiropyran Assemblies: From Nanospheres to Nanorods. *Chem. Asian J.* **11**, 3102–3106 (2016).
66. Krongauz, V. A., Fishman, S. N. & Goldburt, E. S. Quasi-crystals. Growth from photochromic spiropyrans on irradiation in a constant electric field. *J. Phys. Chem.* **82**, 2469–2474 (1978).
67. Florea, L., Scarmagnani, S., Benito-Lopez, F. & Diamond, D. Self-assembled solvato-morphologically controlled photochromic crystals. *Chem. Commun.* **50**, 924–926 (2014).
68. Hammarson, M., Nilsson, J. R., Li, S., Beke-Somfai, T. & Andréasson, J. Characterization of the Thermal and Photoinduced Reactions of Photochromic Spiropyrans in Aqueous Solution. *J. Phys. Chem. B* **117**, 13561–13571 (2013).

69. Shiraishi, Y., Itoh, M. & Hirai, T. Thermal isomerization of spiropyran to merocyanine in aqueous media and its application to colorimetric temperature indication. *Phys. Chem. Chem. Phys.* **12**, 13737 (2010).